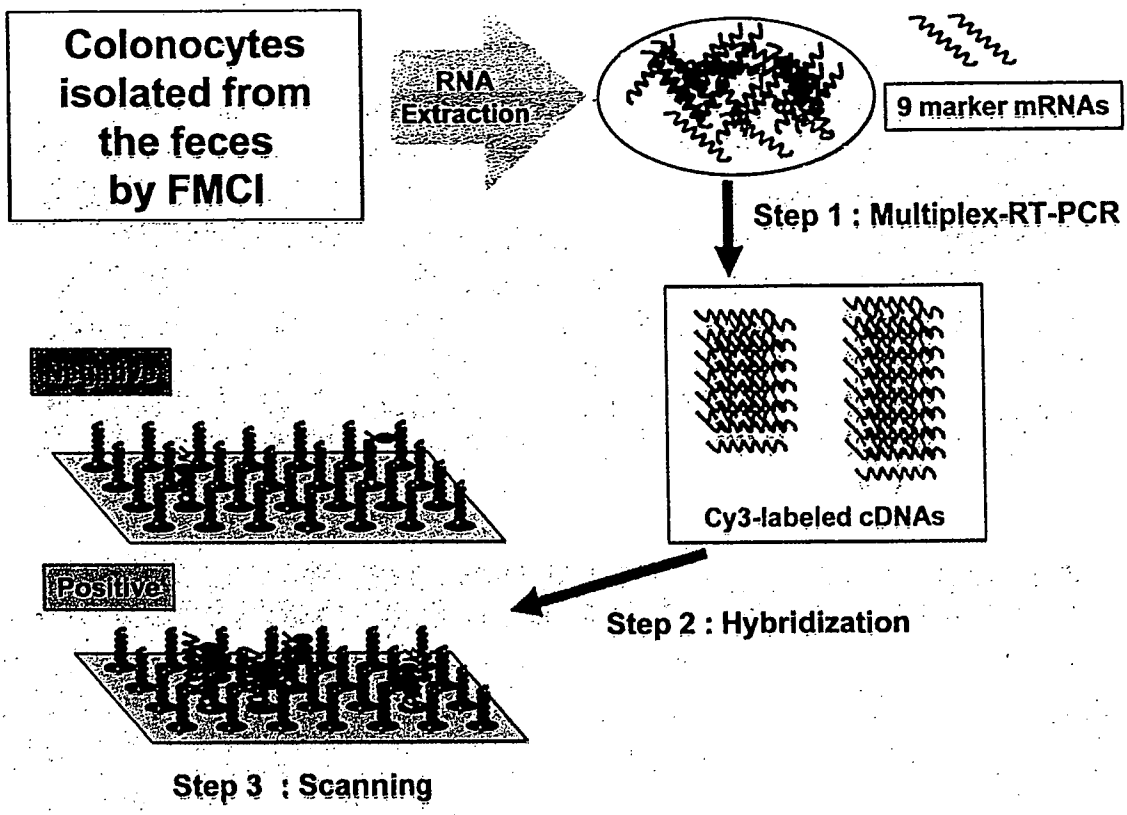

Figure 3. Schematic flow diagram of a focused micoarray assay. Marker mRNAs (PAP, REG1A, DPEP1, SEPP1, RPL27A, ATP1B1, EEF1A1, SFN, and RPS11 mRNAs) were amplified and labeled with Cy3-dUTP by multiplex-RT-PCR among total RNAs from colonocytes isolated by FMCI (step 1) and hybridized to focused micoarray (step 2), followed by fluorescence intensity scanning (step 3).

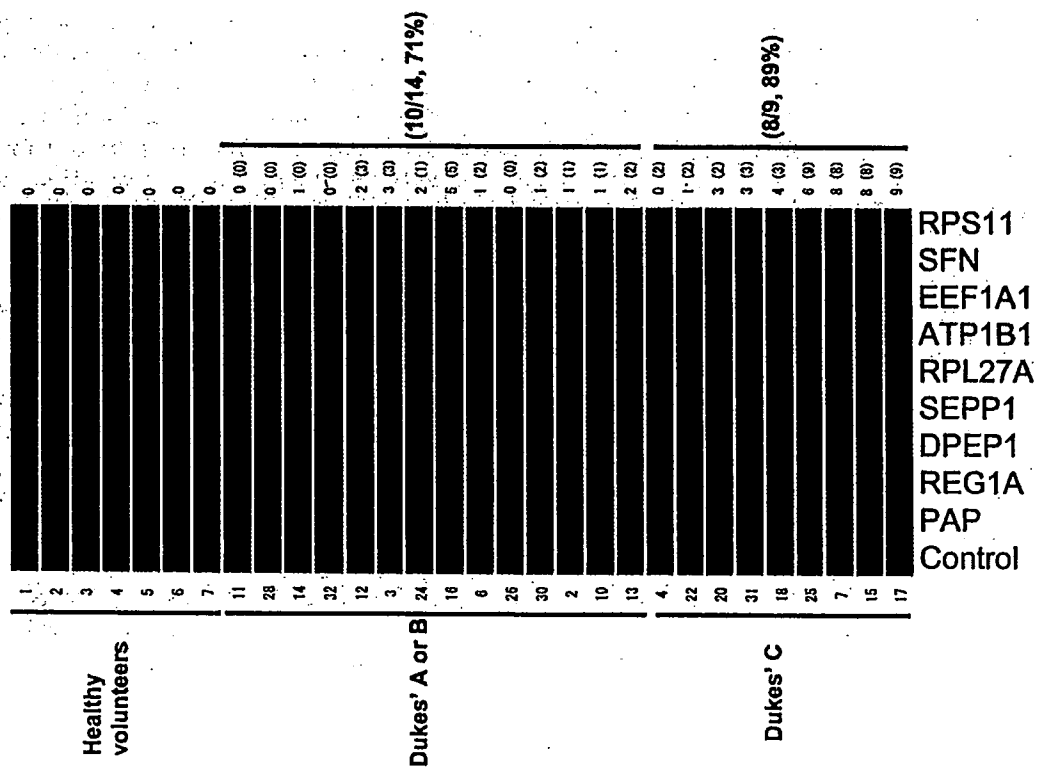

Figure 4. Hybridization image of focused microarray analysis and the number of positive genes in 30 colonocyte RNA samples. The Cy3-labeled cDNAs prepared by multiplex RT-PCR in two tubes were hybridized with 9 gene sequences (PAP, REG1A, DPEP1, SEPP1, RPL27A, ATP1B1, EEF1A1, SFN, and RPS11) on a focused microarray, which was manufactured by our previously developed Bubble Jet Technology with a small modification (25). Hybridization signals and the number of positive genes (right) in the above 23 cancer patient-derived colonocyte RNA samples and 7 healthy volunteer-derived colonocyte RNA samples are shown. In total, a high concordance was observed between focused microarray and RT-PCR. Ten (71%) of the 14 early cancers (Dukes stage A or B) and 8 (89%) of 9 Dukes stage C cancers were detected by the focused microarray analysis. The number of positive genes in RT-PCR are in parentheses (Fig. 2).

materials 6 h to 3 days after evacuation can be obtained if the feces are kept at 4˚C (23). However, if conventional fecal RNA preparation methods without the epithelial cell enrichment process are used for colorectal cancer screening, we have to consider the contamination of blood in the feces, which derives from nonmalignant diseases. Considering the use of such methods, to this end we further provided 56 genes, which were expressed in the cancer patient-derived colonocytes but not in either the healthy volunteer-derived colonocytes or the peripheral blood mixture (Table II). This study suggests that the fecal RNA-based method could be a promising procedure for the detection of early or right-sided colorectal cancers. We recently developed a very effective focused microarray assay for detecting minimal gastric cancer cells in peritoneal washings, demonstrating a specificity and sensitivity equal to or better than cytology in two large specialist hospitals with trained cytologists (26). Therefore, the focused microarray assay could provide an effective imaging tool for mass screening, and our extensive gene list provides useful markers.

Acknowledgments

This study was supported in part by the program for promotion of Fundamental Studies in Health Sciences of the National Institute of Biomedical Innovation (NiBio); in part by a Grant-in-Aid for the Third Comprehensive 10-Year Strategy for Cancer Control and for Cancer Research (16-15) from the Ministry of Health, Labour and Welfare of Japan, and in part by a research and development project of the Industrial Science and Technology Program supported by the New Energy and Industrial Technology Development Organization (NEDO) of Japan. We thank Ayako Nomura and Megumi Sato for their excellent assistance with primer design for RT-PCR.

References

1. Mandel JS, Bond JH, Church TR, Snover DC, Bradley GM, Schman LM and Ederer F: Reducing mortality from colorectal cancer by screening for fecal occult blood. Minnesota Colon Cancer Control Study. N Engl J Med 328: 1365-1371, 1993.
2. Hardcastle JD, Chamberlain JO, Robinson MH, Moss SM, Amar SS, Balfour TW, James PD and Mangham CM: Randomised controlled trial of faecal-occult-blood screening for colorectal cancer. Lancet 348: 1472-1477, 1996.
3. Kronborg O, Fenger C, Olson J, Jorgensen OD and Sondergaard O: Randomized study of screening for colorectal cancer with faecal-occult-blood test. Lancet 348: 1467-1471, 1996.
4. Towler B, Irwig L, Glasziou P, Kewenter J, Weller D and Silagy C: A systematic review of the effects of screening for colorectal cancer using the faecal occult blood test, hemoccult. BMJ 317: 559-565, 1998.
5. Winawer S, Fletcher R, Rex D, Bond J, Burt R, Ferucci J, Ganiats T, Levin T, Woolf S, Johnson D, Kirk L, Litin S and Simmang C: Colorectal cancer screening and surveillance: clinical guidelines and rationale-update based on new evidence. Gastroenterology 124: 544-560, 2003.
6. Mandel JS, Church TR, Bond JH, Ederer F, Geisser MS, Mongin SJ, Snover DC and Schuman LM: The effect of fecal occult-blood screening on the incidence of colorectal cancer. N Engl J Med 343: 1603-1607, 2000.
7. Sidransky D, Tokino T, Hamilton SR, Kinzler KW, Levin B, Frost P and Vogelstein B: Identification of ras oncogene mutations in the stool of patients with curable colorectal tumors. Science 256: 102-105, 1992.
8. Hasegawa Y, Takeda S, Ichii S, Koizumi K, Maruyama M, Fujii A, Ohta H, Nakajima T, Okuda M, Baba S, *et al*: Detection of K-ras mutations in DNAs isolated from feces of patients with colorectal tumors by mutant-allele-specific amplification (MASA). Oncogene 10: 1441-1445, 1995.
9. Smith-Ravin J, England J, Talbot IC and Bodmer W: Detection of c-Ki-ras mutations in faecal samples from sporadic colorectal cancer patients. Gut 36: 81-86, 1995.
10. Eguchi S, Kohara N, Komuta K and Kanematsu T: Mutations of the p53 gene in the stool of patients with resectable colorectal cancer. Cancer 77: 1707-1710, 1996.
11. Nollau P, Moser C, Weinland G and Wagener C: Detection of K-ras mutations in stools of patients with colorectal cancer by mutant-enriched PCR. Int J Cancer 66: 332-336, 1996.
12. Ratto C, Flamini G, Sofo L, Nusera P, Ippliti M, Curigliano G, Ferreti G, Sgambato A, Merico M, Doglietto GB, Cittadini A and Crucitti F: Detection of oncogene mutation from neoplastic colonic cells exfoliated in feces. Dis Colon Rectum 39: 1238-1244, 1996.
13. Deuter R and Muller O: Detection of APC mutations in stool DNA of patients with colorectal cancer by HD-PCR. Hum Mutat 11: 84-89, 1998.
14. Ahlquist DA, Skoletsky JE, Boynton KA, Harrington JJ, Mahoney DW, Pierceall WE, Thibodeau SN and Shuber AP: Colorectal cancer screening by detection of altered human DNA in stool: feasibility of a multitarget assay panel. Gastroenterology 119: 1219-1227, 2000.
15. Dong SM, Traverso G, Johnson C, Geng L, Favis R, Boynton K, Hibi K, Goodman SN, D'Allessio M, Paty P, Hamilton SR, Sidransky D, Barany F, Levin B, Shuber A, Kinzler KW, Vogelstein B and Jen J: Detecting colorectal cancer in stool with the use of multiple genetic targets. J Natl Cancer Inst 93: 858-865, 2001.
16. Rengucci C, Maiolo P, Saragoni L, Zoli W, Amadori D and Calistri D: Multiple detection of genetic alterations in tumors and stool. Clin Cancer Res 7: 590-593, 2001.
17. Traverso G, Shuber A, Olsson L, Levin B, Johnson C, Hamilton SR, Boynton K, Kinzler KW and Vogelstein B: Detection of proximal colorectal cancers through analysis of faecal DNA. Lancet 359: 403-404, 2002.
18. Traverso G, Shuber A, Levin B, Levin B, Johnson C, Hamilton SR, Boynton K, Kinzler KW and Vogelstein B: Detection of APC mutations in fecal DNA from patients with colorectal tumors. N Engl J Med 346: 311-320, 2002.
19. Boynton KA, Summerhayes IC, Ahlquist DA and Shuber AP: DNA integrity as a potential marker for stool-based detection of colorectal cancer. Clin Chem 49: 1058-1065, 2003.
20. Matsumura Y and Tarin D: Significance of CD44 gene products for cancer diagnosis and disease evaluation. Lancet 340: 1053-1058, 1992.
21. Mastumura Y, Hanbury D, Smith J and Tarin D: Non-invasive detection of malignancy by identification of unusual CD44 gene activity in exfoliated cancer cells. BMJ 308: 619-624, 1994.
22. Yamao T, Matsumura Y, Shimada Y, Moriya Y, Sugihara K, Akasu T, Fujita S and Kakizoe T: Abnormal expression of CD44 variants in the exfoliated cells in the feces of patients with colorectal cancer. Gastroenterology 114: 1196-1205, 1998.
23. Matsushita H, Matsumura Y, Moriya Y, Akasu T, Fujita S, Yamamoto S, Onouchi S, Saito N, Sugito M, Ito M, Kozu T, Minowa T, Nomura S, Tsunoda H and Kakizoe T: A new method for isolating colonocytes from naturally evacuated feces and its clinical application to colorectal cancer diagnosis. Gastroenterology 129: 1918-1927, 2005.
24. Mori K, Aoyagi K, Ueda T, Danjoh I, Tsubosa Y, Yanagihara K, Matsuno Y, Sasako M, Sakamoto H, Mafune K, Kaminishi M, Yoshida T, Terada M and Sasaki H: Highly specific marker genes for detecting minimal gastric cancer cells in cytology negative peritoneal washings. Biochem Biophys Res Commun 313: 931-937, 2004.
25. Okamoto T, Suzuki T and Yamamoto N: Microarray fabrication with covalent attachment of DNA using Bubble Jet Technology. Nat Biotech 18: 438-441, 2000.
26. Mori K, Suzuki T, Uozaki H, Nakanishi H, Ueda T, Matsuno Y, Kodera Y, Sakamoto H, Yamamoto N, Sasako M, Kaminishi M and Sasaki H: Detection of minimal gastric cancer cells in peritoneal washings by focused microarray analysis with multiple markers: clinical implications. Ann Surg Oncol 14: 1694-1702, 2007.

Novel SN-38–Incorporated Polymeric Micelle, NK012, Strongly Suppresses Renal Cancer Progression

Makoto Sumitomo,[1] Fumiaki Koizumi,[2] Takako Asano,[1] Akio Horiguchi,[1] Keiichi Ito,[1] Tomohiko Asano,[1] Tadao Kakizoe,[3] Masamichi Hayakawa,[1] and Yasuhiro Matsumura[4]

[1]Department of Urology, National Defense Medical College, Tokorozawa, Saitama, Japan; [2]Shien-Lab, Medical Oncology, National Cancer Center Hospital; [3]National Cancer Center, Tokyo, Japan; and [4]Investigative Treatment Division, Research Center for Innovative Oncology, National Cancer Center Hospital East, Chiba, Japan

Abstract

It has been recently reported that NK012, a 7-ethyl-10-hydroxy-camptothecin (SN-38)–releasing nanodevice, markedly enhances the antitumor activity of SN-38, especially in hypervascular tumors through the enhanced permeability and retention effect. Renal cell carcinoma (RCC) is a typical hypervascular tumor with an irregular vascular architecture. We therefore investigated the antitumor activity of NK012 in a hypervascular tumor model from RCC. Immunohistochemical examination revealed that Renca tumors contained much more CD34-positive neovessels than SKRC-49 tumors. Compared with CPT-11, NK012 had significant antitumor activity against both bulky Renca and SKRC-49 tumors. Notably, NK012 eradicated rapid-growing Renca tumors in 6 of 10 mice, whereas it failed to eradicate SKRC-49 tumors. In the pulmonary metastasis treatment model, an enhanced and prolonged distribution of free SN-38 was observed in metastatic lung tissues but not in nonmetastatic lung tissues after NK012 administration. NK012 treatment resulted in a significant decrease in metastatic nodule number and was of benefit to survival. Our study shows the outstanding advantage of polymeric micelle-based drug carriers and suggests that NK012 would be effective in treating disseminated RCCs with irregular vascular architectures. [Cancer Res 2008;68(6):1631–5]

Introduction

Passive targeting of the drug delivery system is suited to combating the pathophysiologic characteristics present in many solid tumors: hypervascularity, irregular vascular architecture, potential for secretion of vascular permeability factors, and the absence of effective lymphatic drainage that prevents efficient clearance of macromolecules. These characteristics, unique to solid tumors, are believed to be the basis of the enhanced permeability and retention (EPR) effect (1). Polymeric micelle-based anticancer drugs have recently been developed (2, 3), and some were put under evaluation for clinical trials (4, 5).

7-Ethyl-10-hydroxy-camptothecin (SN-38), a biological active metabolite of irinotecan hydrochloride (CPT-11), has potent antitumor activity, but has not been used clinically because it is a water-insoluble drug. It has been recently shown that novel SN38-incorporated polymeric micelles, NK012, have the potential to allow effective sustained release of SN-38 inside a tumor and possess potent antitumor activities especially in a vascular endothelial growth factor (VEGF)–secreting hypervascular tumor (6), because the supramolecular structures of NK012 which enable SN-38 to accumulate in the target tissue are based on the EPR effect (1).

Renal cell carcinoma (RCC) is a typical hypervascular tumor with an irregular vascular architecture. We therefore conducted an investigation to determine whether NK012 would be effective in treating RCC by using established RCC tumor models with pulmonary metastasis.

Materials and Methods

Drugs and cells. CPT-11 was purchased from Yakult Honsha Co., Ltd. SN-38 and NK012 was prepared and supplied by Nippon Kayaku Co., Ltd. (6). Five human RCC lines (SKRC-49, Caki-1, 769P, 786O, and KU19-20) and murine Renca cells were maintained in DMEM or MEM supplemented with 2 mmol/L glutamine, 1% nonessential amino acids, 100 units/mL streptomycin and penicillin, and 10% FCS.

***In vitro* growth inhibition assay.** The growth inhibitory effects of NK012, SN-38, and CPT-11 were examined with a 3-(4, 5-dimethylthiazol-2-yl)-2, 5-diphenyltetrazolium bromide (MTT) assay, as described previously (6).

***In vivo* growth inhibition assay.** The animal experimental protocols were approved by the Committee for Ethics of Animal Experimentation, and the experiments were conducted in accordance with the Guidelines for Animal Experiments in the National Cancer Center. Athymic nude mice (3–4 wk old) were maintained in a laminar air flow cabinet under aseptic conditions. 10^7 RCC cells were s.c. injected into the backs of the mice. NK012 at doses of 10 mg/kg/d or 20 mg/kg/d and CPT-11 at doses of 15 mg/kg/d or 30 mg/kg/d were given i.v. on days 0 (when tumors were allowed to grow until they became massive in size, around 1.5 cm), 4, and 8. Tumor volume was determined by direct measurement with calipers and calculated as $\pi/6 \times$ (large diameter) $\times$ (small diameter)^2.

Assessment of treatment effects of NK012 on murine pulmonary metastasis model. A total of 1×10^5 Renca cells were inoculated into male BALB/c mice via the tail vein. The mice were randomly divided into three groups of 10. NK012 at dose of 20 mg/kg/d and CPT-11 at dose of 30 mg/kg/d were given i.v. on days 0 (7 d after inoculation), 4, and 8. After that, the mice were sacrificed, their lungs were stained intratracheally with 15% India black ink solution, and the number of metastatic nodules in each mouse was counted. To determine the effect of NK012 on survival, an identical experiment to the one described above was done. After treatment, mice were maintained until each animal showed signs of morbidity (i.e., over 10% weight loss compared with untreated controls), at which point they were sacrificed. Kaplan-Meier analysis was done to determine the effect on time to morbidity, and statistical differences were ranked according to a Mantel-Cox log-rank test using the StatView 5.0 software package.

Histologic and immunohistochemical analysis. Histologic sections were taken from Renca tumor tissues. After extirpation, tissues were fixed with 3.9% formalin in PBS (pH 7.4), and the subsequent preparations and H&E staining were performed by Tokyo Histopathological Laboratory Co.,

Requests for reprints: Yasuhiro Matsumura, Investigative Treatment Division, Research Center for Innovative Oncology, National Cancer Center Hospital East, 6-5-1 Kashiwanoha, Kashiwa City, Chiba 277-8577, Japan. Phone: 81-4-7134-6857; Fax: 81-4-7134-6857; E-mail: yhmatsum@east.ncc.go.jp.

doi:10.1158/0008-5472.CAN-07-6532

Table 1. *In vitro* growth inhibitory activity of SN-38, NK012, and CPT-11 in RCC lines (MTT assay)

Cell line	IC_{50} (μmol/L)		
	SN-38	NK012*	CPT-11
SKRC-49	0.0064 ± 0.005	0.011 ± 0.008	4.14 ± 0.45
Caki-1	0.0062 ± 0.009	0.032 ± 0.006	8.45 ± 0.85
769P	0.015 ± 0.007	0.085 ± 0.014	34.54 ± 3.76
786O	0.031 ± 0.007	0.12 ± 0.012	28.14 ± 1.21
KU19-20	0.10 ± 0.006	0.34 ± 0.014	32.65 ± 1.25
Renca	0045 ± 0.005	0.0096 ± 0.008	2.26 ± 0.05

*The dose of NK012 is expressed as a dose equivalent to SN-38.

Ltd. Monoclonal anti-CD34 antibody (HyCult Biotechnology) was used to detect the tumor blood vessels. CD34-positive neovessels were counted in 10 high-power fields (×400) by two independent investigators who operated in a blinded fashion.

Assay for free (polymer-unbound) SN-38 in lung tissues. The Renca pulmonary metastasis model described above was used for the analysis of the biodistribution of NK012 and CPT-11. Ten days after Renca inoculation, NK012 (20 mg/kg) or CPT-11 (30 mg/kg) was given i.v. to the mice. The mice were sacrificed at 0, 24, 48, and 72 h after administration, and lung samples were taken and stored at −80°C until analysis. We prepared control mice without Renca inoculation as the nonmetastatic model; NK012 was administrated as well, and lung samples were stored. Samples were then homogenized on ice using a Digital homogenizer (Iuchi) and suspended in the mixture of 100 mmol/L glycine-HCl buffer (pH 3)/methanol (1:1, v/v) at a concentration of 5% w/w. Proteins were precipitated with an ice-cold mixture of 1 mmol/L H_3PO_4/MeOH/H_2O (1:1:4, v/v/v) containing camptothecin as an I.S. The sample was vortexed for 10 s and filtered through a MultiScreen Solvinert (Millipore Corporation), and the concentration of free SN-38 in the aliquots of the homogenates (100 μL) was determined using the high-performance liquid chromatography method (6).

Statistical analysis. Data were expressed as mean ± SD. Significance of differences was calculated using the unpaired *t* test with repeated measures of StatView 5.0. $P < 0.05$ was regarded as statistically significant.

Results and Discussion

We first evaluated *in vitro* cellular sensitivity of RCC lines to SN-38, NK012, and CPT-11. The IC_{50} values of each agent for RCC lines are shown in Table 1. NK012 exhibited higher cytotoxic effect against each cell line compared with CPT-11 (96-fold to 406-fold sensitive).

It is essential to elucidate the correlation between the effectiveness of micellar drugs and tumor hypervascularity and hyperpermeability. Gross evaluation of those RCC tumors s.c. injected into the backs of mice revealed that Renca tumors were more reddish and grew faster than SKRC-49 tumors, and immunohistochemical examination showed that Renca tumors contained much more CD34-positive neovessels than SKRC-49 tumors (Fig. 1).

We allowed the tumors to grow until they became massive, around 1.5 cm, and then initiated treatment. A striking decrease in Renca tumor volume was observed on day 15 in mice treated with NK012 at 20 mg/kg/d compared with the untreated control (Fig. 2*A*). Renca bulky masses completely disappeared on day 21 in 6 of 10 mice treated with NK012 at 20 mg/kg/d. On the other hand, Renca tumors in mice treated with CPT-11 at 30 mg/kg/d were not eradicated and rapidly regrew after a partial response at day 15. An approximate 10% body weight loss occurred in mice treated with NK012 20 mg/kg, compared with the untreated controls, but there was no significant difference in comparison with tumor-free mice treated with NK012, suggesting that the decrease in body weight was likely to be due to tumor shrinkage rather than toxic effects. We next compared the antitumor activities of the NK012 and CPT-11 treatment in SKRC-49 and Renca tumors. The SKRC-49 tumor volume in mice treated with NK012 at 20 mg/kg/d on day 21 was over 70% smaller than in the untreated controls on day 21 and ~50% smaller than in mice on day 0 (Fig. 2*B*). However, the SKRC-49 tumors were not eradicated in mice treated with NK012. Considering that equivalent *in vitro* growth inhibitory effects by NK012 were observed for SKRC-49 and Renca cells (Table 1), our results suggest that the antitumor activity of NK012 *in vivo* might be affected by tumor environment factors, such as tumor vascularity.

We next examined the distribution of free SN-38 in the metastatic or nonmetastatic (no inoculation of Renca cells) lung tissues after administration of NK012 or CPT-11. In the case of NK012 administration in mice with lung metastasis, free SN-38 was detectable at the concentration of >100 ng/g in metastatic lung tissues with a typical microvascular architecture (Fig. 3*A*) even at 72 hours after administration, whereas the concentrations of free SN-38 in nonmetastatic lung tissues after NK012 administration were much lower than those in metastatic lung tissues after treatment with NK012 (significant at 24, 48, and 72 hours; $P < 0.05$;

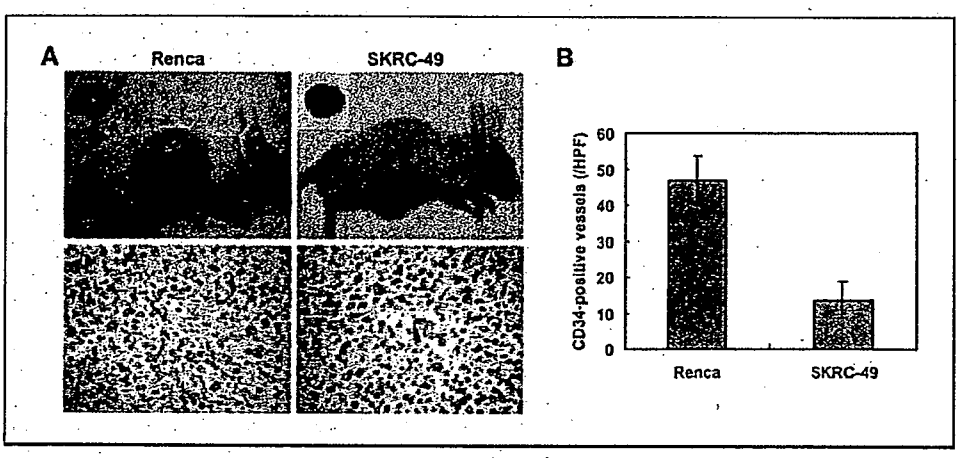

Figure 1. Comparison of tumor angiogeneses of Renca and SKRC-49 in athymic nude mice. *A*, representative photographs of massive tumors developed from Renca and SKRC-49 at 28 d after s.c. injection (inoculation). Immunohistochemical (CD34, ×400) examinations for each tumor are shown. *B*, tumor neovascularization in each tumor was quantified by counting CD34-positive neovessels. *Bars*, SD. Experiments were repeated twice with similar results.

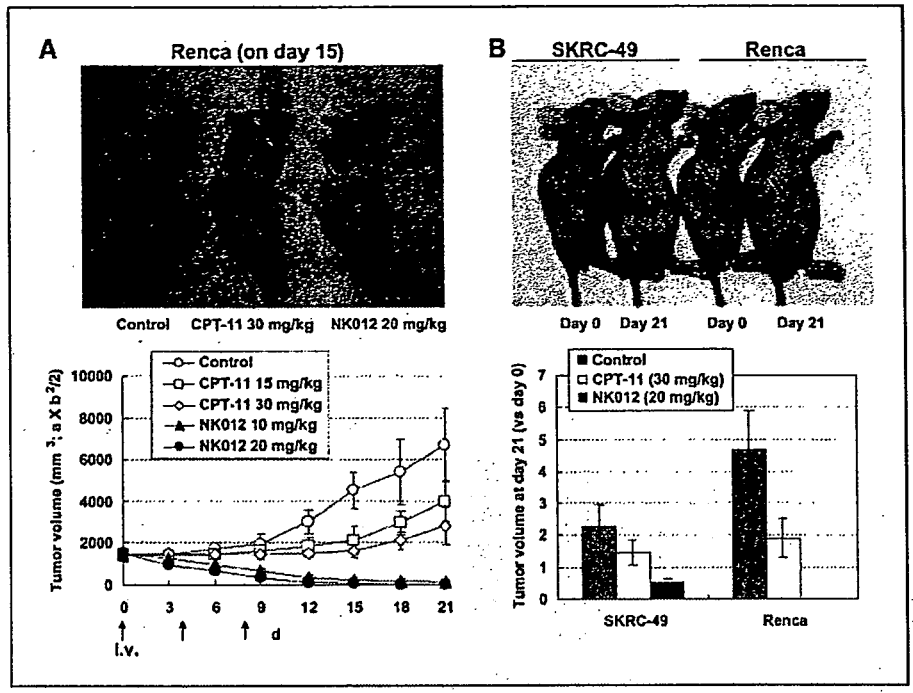

Figure 2. Growth-inhibitory effect of NK012 and CPT-11 on bulky RCC tumors. I.v. administration of NK012 or CPT-11 was started when the mean tumor volumes of groups reached a massive 1,500 mm^3. The mice were divided into test groups as indicated. *A*, representative of each group at day 15 in the Renca allograft model. *Arrows*, Renca allografts (*top*). Time profile of tumor volume in mice treated with NK012 or CPT-11 at indicated doses (*bottom*). Each group consisted of 10 mice. *Bars*, SD. *B*, the comparison of antitumor activities of CPT-11 and NK012 in SKRC-49 xenografts and Renca allografts. Representative of mice treated with NK012 at day 0 and day 21. Experiments were repeated twice with similar results. The mice at day 0 in the photograph belong to the group in the second experiment which started just at day 21 of the first experiment. *Arrows*, tumor grafts. The relative tumor volume values at day 21 to those at day 0 in each group set to 1 (*bottom*). Each group consisted of 10 mice.

Fig. 3*B*). On the other hand, the concentrations of free SN-38 after administration of CPT-11 were almost negligible in metastatic lung tissues at all time points (data not shown). These results strongly suggest that SN-38 could be selectively released from NK012 and maintained in metastatic Renca tumor tissues.

Deviating from the ordinary experimental pulmonary metastasis prevention model, we initiated treatment 7 days after inoculation (day 0) when multiple lung nodules derived from Renca were observed in all mice in our preliminary study (Fig. 4*A*). On day 21, there was no significant difference between the mean number of metastatic nodules in the control group (287 ± 56 nodules, $n = 10$) and in the group receiving CPT-11 treatment (236 ± 59 nodules, $n = 10$). Significant treatment effects were found, however, in the group receiving NK012 treatment (32 ± 18 nodules, $n = 10$) on day 21 compared with the control group on day 21 ($P < 0.0001$). Notably, a dramatic decrease in metastatic nodule number was observed in the NK012 treatment group on day 21 compared with the control group on day 0 (126 ± 23 nodules, $n = 10$, $P < 0.001$; Fig. 4*A*). Kaplan-Meier analysis showed that a significant survival benefit was obtained in the NK012 treatment group compared with

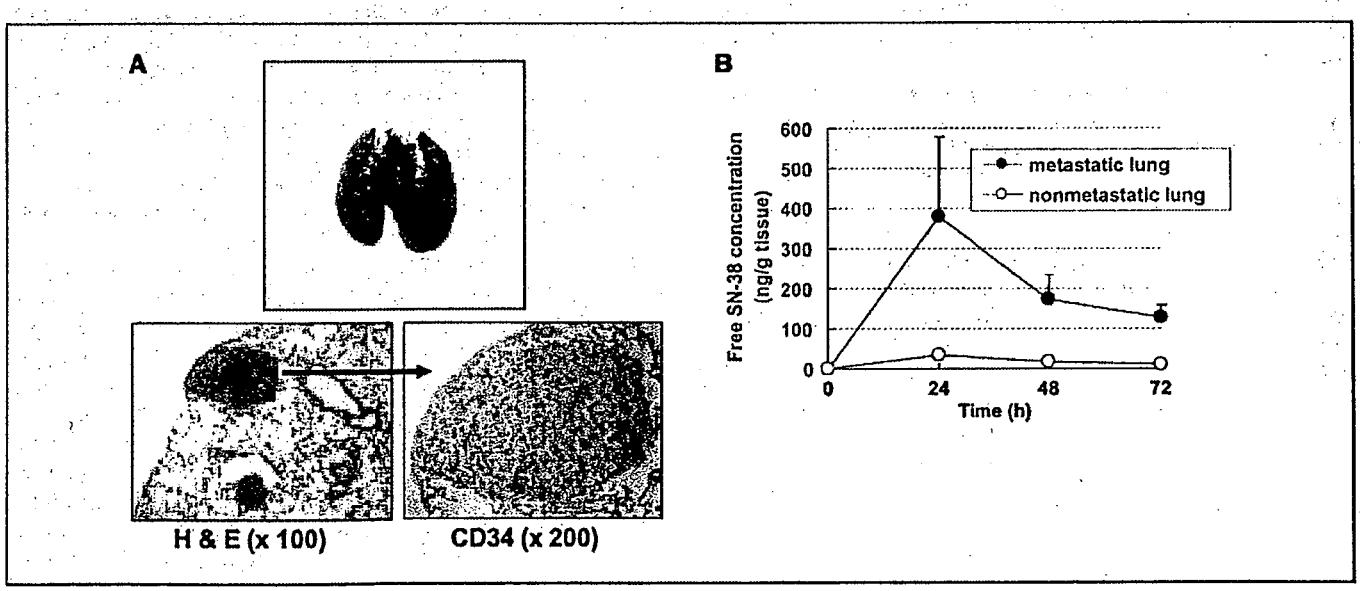

Figure 3. Pulmonary metastasis of Renca cells and lung tissue distribution of free SN-38 after administration of NK012 and CPT-11. *A*, gross appearances of pulmonary metastasis observed 7 d after Renca inoculation (*top*). Multiple metastatic nodules and neovascularization in metastatic lung tumor lesion (*bottom*). *B*, time profile of free SN-38 concentration in metastatic or nonmetastatic lung tissues in mice treated with NK012 (20 mg/kg/d). *Bars*, SD. Experiments were performed in tetraplicate.

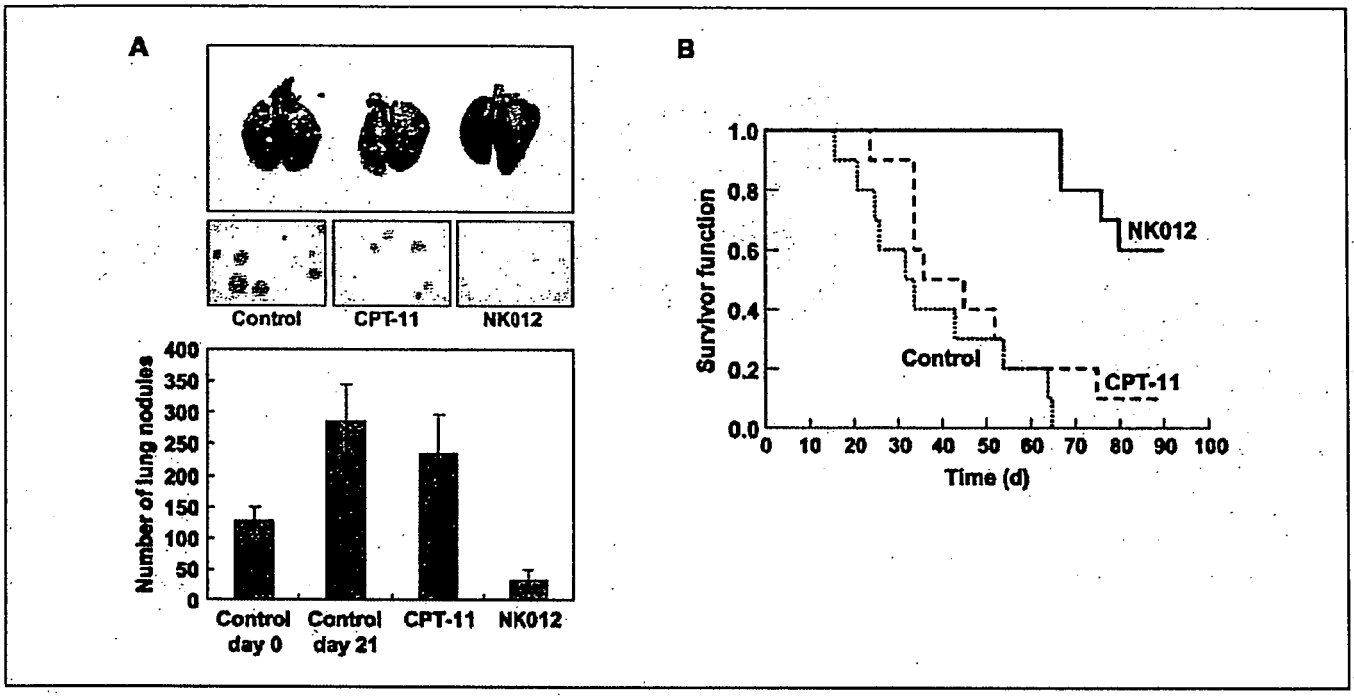

Figure 4. Treatment effect of NK012 on established pulmonary metastasis and survival. NK012 (20 mg/kg/d) and CPT-11 (30 mg/kg/d) were given i.v. to mice with established pulmonary metastasis on days 0 (7 d after Renca inoculation), 4, and 8. *A*, gross and histologic appearances of pulmonary metastases at day 21 (*top*). The metastatic nodules in each mouse were counted. Each group consisted of five mice. *B*, mice were maintained for 90 d after each treatment and survival was assessed by a Kaplan-Meier analysis. Each group consisted of five mice. Experiments were repeated twice with similar results.

the control group ($P < 0.001$), but no significant survival benefit was obtained in CPT-11 treatment group ($P = 0.239$; Fig. 4*B*). Although no severe toxic effects were observed in any mouse treated with NK012, 3 of 10 mice treated with NK012 were sacrificed during the observation period according to the 'Guidelines for Animal Experiments because their body weights had become 10% lower than those of the other mice. However, the sacrificed mice were a little bit smaller than others when they started treatment, and they showed no disseminated lung metastasis (data not shown).

Our results presented here strongly support recent findings reported by us that the macromolecular drug distribution throughout the tumor site was enhanced by the hypervascularity and hyperpermeability, and subsequently higher antitumor activity was achieved (6). We assume that conventional low molecular size anticancer agents almost disappear from the bloodstream without being subjected to the EPR effect before they can reach the target organs (solid tumor). The clinical importance of angiogenesis in human tumors has been shown in several reports indicating a positive relationship between the blood vessel density in the tumor mass and poor prognosis with chemoresistance in patients with various cancers (7–9). Furthermore, recent reports showing that anticancer agents were less active against VEGF-overexpressing tumors (10, 11) may support the idea that low-molecular drugs are not so effective in the treatment of solid tumors which are rich in blood vessels.

Our study thus far has several limitations about clarifying whether extensive angiogenesis in the tumor is an essential determinant for the susceptibility to NK012. In our ongoing study, we found that NK012 also has a striking antitumor activity against some hypovascular tumor models of human pancreatic cancer xenografts.[5] It also remains unclear whether NK012 possesses strong antitumor activity in other metastatic sites besides the lung. It is known that the EPR effect is affected by various permeability factors, such as bradykinin (12), nitric oxide (13), and various cytokines independent of VEGF and hypervascularity (14). Among solid tumors with rapid progression potential, irregularity occurs not only in blood flow and vascular density, but also in the vascular network and anatomic architecture (15, 16), suggesting that EPR effect may be predominantly promoted in rapid-progressive tumor phenotypes and influenced by organ-specific tumor microenvironment. Hoffman and coworkers (17, 18) have developed a technique of surgical orthotopic implantation (SOI) with more clinical features of systemic and aggressive metastases than our conventional animal models. Further preclinical studies using such models as SOI might clarify cancer phenotypes and metastatic organs to which we can apply NK012 more precisely.

The results of chemotherapy in RCCs have been disappointing, as indicated by the low response proportions. However, clinical trials using gemcitabine-containing regimens have been encouraging, with major responses occurring in 5% to 17% of patients (19, 20), suggesting the possibility that chemotherapy is promising as a modality for RCC therapy if anticancer agents can be selectively delivered, released, and maintained around tumor tissues. Our current report highlights the advantages of polymeric micelle-based drug carriers like NK012 as promising modalities for treatment, rather than prevention, of disseminated RCCs with abnormal vascular architecture. The results of our ongoing phase-I

[5] Y. Saito, M. Yasumaga, J. Kuroda, Y. Koga, and Y. Matsumura. Unpublished data.

clinical trial and future phase-II trials of NK012 in patients with advanced solid tumors including RCC might meet or even exceed our expectations.

Acknowledgments

Received 12/10/2007; revised 1/25/2008; accepted 1/31/2008.

Grant support: Grant-in-aid from 3rd Term Comprehensive Control Research for Cancer, Ministry of Health, Labor and Welfare (Y. Matsumura) and Scientific Research on Priority Areas from the Ministry of Education, Culture, Sports, Science and Technology (Y. Matsumura).

The costs of publication of this article were defrayed in part by the payment of page charges. This article must therefore be hereby marked *advertisement* in accordance with 18 U.S.C. Section 1734 solely to indicate this fact.

We thank H. Miyatake and N. Mie for their technical assistance and K. Shiina for her secretarial assistance.

References

1. Matsumura Y, Maeda H. A new concept for macromolecular therapeutics in cancer chemotherapy: mechanism of tumoritropic accumulation of proteins and the antitumor agent smancs. Cancer Res 1986;46:6387–92.
2. Yokoyama M, Miyauchi M, Yamada N, et al. Characterization and anticancer activity of the micelle-forming polymeric anticancer drug adriamycin-conjugated poly(ethylene glycol)-poly(aspartic acid) block copolymer. Cancer Res 1990;50:1693–700.
3. Kataoka K, Harada A, Nagasaki Y. Block copolymer micelles for drug delivery: design, characterization and biological significance. Adv Drug Deliv Rev 2001;47:113–31.
4. Matsumura Y, Hamaguchi T, Ura T, et al. Phase I clinical trial and pharmacokinetic evaluation of NK911, a micelle-encapsulated doxorubicin. Br J Cancer 2004;91:1775–81.
5. Hamaguchi T, Kato K, Yasui H, et al. A phase I and pharmacokinetic study of NK105, a paclitaxel-incorporating micellar nanoparticle formulation. Br J Cancer 2007;97:170–6.
6. Koizumi F, Kitagawa M, Negishi T, et al. Novel SN-38-incorporating polymeric micelles, NK012, eradicate vascular endothelial growth factor-secreting bulky tumors. Cancer Res 2006;66:10048–56.
7. Gasparini G, Harris AL. Clinical importance of the determination of tumor angiogenesis in breast carcinoma: much more than a new prognostic tool. J Clin Oncol 1995;13:765–82.
8. Takahashi Y, Kitadai Y, Bucana CD, Cleary KR, Ellis LM. Expression of vascular endothelial growth factor and its receptor, KDR, correlates with vascularity, metastasis, and proliferation of human colon cancer. Cancer Res 1995;55:3964–8.
9. Williams JK, Carlson GW, Cohen C, Derose PB, Hunter S, Jurkiewicz MJ. Tumor angiogenesis as a prognostic factor in oral cavity tumors. Am J Surg 1994;168:373–80.
10. Natsume T, Watanabe J, Koh Y, et al. Antitumor activity of TZT-1027 (Soblidotin) against vascular endothelial growth factor-secreting human lung cancer *in vivo*. Cancer Sci 2003;94:826–33.
11. Zhang L, Hannay JA, Liu J, et al. Vascular endothelial growth factor overexpression by soft tissue sarcoma cells: implications for tumor growth, metastasis, and chemoresistance. Cancer Res 2006;66:8770–8.
12. Matsumura Y, Maruo K, Kimura M, Yamamoto T, Konno T, Maeda H. Kinin-generating cascade in advanced cancer patients and *in vitro* study. Jpn J Cancer Res 1991;82:732–41.
13. Wu J, Akaike T, Hayashida K, et al. Identification of bradykinin receptors in clinical cancer specimens and murine tumor tissues. Int J Cancer 2002;98:29–35.
14. Maeda H, Fang J, Inutsuka T, Kitamoto Y. Vascular permeability enhancement in solid tumor: various factors, mechanisms involved and its implications. Int Immunopharmacol 2003;3:319–28.
15. Suzuki M, Takahashi T, Sato T. Medial regression and its functional significance in tumor-supplying host arteries. A morphometric study of hepatic arteries in human livers with hepatocellular carcinoma. Cancer 1987;59:444–50.
16. Skinner SA, Tutton PJ, O'Brien PE. Microvascular architecture of experimental colon tumors in the rat. Cancer Res 1990;50:2411–7.
17. An Z, Jiang P, Wang X, Moossa AR, Hoffman RM. Development of a high metastatic orthotopic model of human renal cell carcinoma in nude mice: benefits of fragment implantation compared to cell-suspension injection. Clin Exp Metastasis 1999;17:265–70.
18. Hoffman RM. Orthotopic metastatic mouse models for anticancer drug discovery and evaluation: a bridge to the clinic. Invest New Drugs 1999;17:343–59.
19. Rini BI, Vogelzang NJ, Dumas MC, Wade JL III, Taber DA, Stadler WM. Phase II trial of weekly intravenous gemcitabine with continuous infusion fluorouracil in patients with metastatic renal cell cancer. J Clin Oncol 2000;18:2419–26.
20. Nanus DM, Garino A, Milowsky MI, Larkin M, Dutcher JP. Active chemotherapy for sarcomatoid and rapidly progressing renal cell carcinoma. Cancer 2004;101:1545–51.

Ultrasound in Med. & Biol., Vol. 34, No. 3, pp. 425–434, 2008

0301-5629/08/$–see front matter

doi:10.1016/j.ultrasmedbio.2007.09.004

● *Original Contribution*

HERPES SIMPLEX VIRUS THYMIDINE KINASE-MEDIATED SUICIDE GENE THERAPY USING NANO/MICROBUBBLES AND ULTRASOUND

ATSUKO AOI,*† YUKIKO WATANABE,* SHIRO MORI,‡ MASAHIKO TAKAHASHI,† GEORGES VASSAUX,§‖ and TETSUYA KODAMA*

*Biomedical Engineering Research Organization, Tohoku University, †Graduate School of Dentistry, Tohoku University, ‡Tohoku University Hospital, Sendai, Japan; and §INSERM CIC-004, ‖Institut des maladies de l'Appareil Digestif, CHU Hotel Dieu, Nantes, France

(*Received* 12 *January* 2007, *revised* 25 *June* 2007, *in final form* 5 *September* 2007)

Abstract—A physical method using ultrasound (US) and nano/microbubbles (NBs) can deliver exogenous molecules noninvasively into a specific target site. In this study, we evaluated the application of this technology to cancer gene therapy using prodrug activation therapy. Low-intensity pulsed ultrasound (1 MHz; 1.3 W/cm^2) and NBs were used to transduce the herpes simplex thymidine kinase (HSV*tk*) gene *in vitro*, leading to gene transfer. The addition of ganciclovir (GCV) to the transduced cells led to HSV*tk*/GCV-dependent cell death mediated by apoptosis. This technology was then assessed *in vivo*, using mice bearing subcutaneous tumors (1 MHz; 3.0 W/cm^2). Gene transfer to the tumor, measured by luciferase activity, was transient, with a peak of expression 24 h after transduction, and decreased at 48 h, demonstrating the transient nature of US/NB-mediated gene transfer. The therapeutic potential of this approach was evaluated through repeated intratumoral gene delivery using US/NB-mediated transfer of the HSV*tk* gene, followed by recurrent administration of GCV, using two different experimental treatment protocols. In both cases, dramatic reductions of the tumor size by a factor of four were observed. Altogether, these data demonstrate the potential of US/NB as a new physical gene delivery method for cancer gene therapy. (E-mail: kodama@tubero.tohoku.ac.jp) © **2008 World Federation for Ultrasound in Medicine & Biology.**

Key Words: **Membrane permeability, *In-vivo* imaging, Molecular delivery, Cancer gene therapy.**

INTRODUCTION

Cancer therapy based on gene delivery requires highly efficient molecular delivery methods into a specific target site. One of the physical methods of gene delivery exploits nano/microbubbles (NBs) combined with ultrasound (US). Nano/microbubbles are encapsulated gas bubbles with a radius of <5 μm. The shell membrane consists of albumin, lipid or polymer. The inside gas comprises either air or perfluorocarbons (large molecules have a small diffusion efficiency into liquid, resulting in increased bubble life time) (Chomas et al. 2001; Harvey et al. 2001). These bubbles are not only used as US contrast agent to identify and delineate cardiac anatomy, such as thrombi or clot formation, but they are also used for evaluation of blood pool and blood flow at the microvascular level (Lindner 2004). The mechanical index (MI, defined as the peak negative pressure divided by the square root of the US frequency) of US used in clinical application is 0.05 to 1.9 (McCulloch et al. 2000) and NBs collapse at MI = 0.3 to 0.5 (Ammi et al. 2006; Chen et al. 1995; Wu and Tong 1998). The impulsive pressures generated by either the collapse of NBs or cavitation bubbles created by the collapse of NBs are able to induce a transient permeabilization of cells, followed by the entry of exogenous molecules into cells. This method is not toxic and nonimmunogenic and can be combined with chemotherapy (Pitt et al. 2004).

Suicide gene therapy involves transfer into cancer cells of a gene capable of converting nontoxic prodrugs into cytotoxic drugs. One of the most common approaches uses the herpes simplex virus thymidine kinase (HSV*tk*) gene combined with the prodrug ganciclovir (GCV). The nucleoside analogue GCV is phosphorylated 1,000 times less efficiently by eukaryotic thymidine kinases and experimentally, *in vivo*, GCV is only phosphorylated by cells producing the virus enzyme HSV*tk*

Address correspondence to: Tetsuya Kodama, Ph.D., Professor, Biomedical Engineering Research Organization, Tohoku University, 2–1 Seiryo-machi, Aoba-ku, Sendai 980–8575, Japan. E-mail: kodama@tubero.tohoku.ac.jp

(Keller et al. 1981; Oliver et al. 1985). The product of the reaction (GCV-MP) is then further phosphorylated to GCV-diphosphate (GCV-DP) and GCV-triphosphate (GCV-TP) by endogenous cellular kinases. GCV-TP inhibits competitively the incorporation of dGTP into DNA (Mesnil and Yamasaki 2000), resulting in cell death (Fillat et al. 2003; Mesnil and Yamasaki 2000). Apoptosis has been suggested to be involved in the cell death, which may occur by a pathway independent of p53 (Wallace et al. 1996). In fact, it has been reported that cell lines with mutant p53 expressing HSV*tk* were not resistant to GCV (Vassaux and Martin-Duque 2004; Wallace et al. 1996; Yoon et al. 1999). Cytotoxicity is observed not only in HSV*tk*-positive cells but also in neighboring HSV*tk*-negative cells as a result of the bystander effect. HSV*tk*-negative cells show cytotoxicity *in vitro* when the population of cultured cells contained only 10% HSV*tk*-positive cells (Freeman et al. 1993). This bystander effect is regarded as a transfer phenomenon of the toxic metabolites of GCV from HSV*tk*-positive cells to HSV*tk*-negative cell, in which gap junctional intercellular communication (GJIC) appears crucial.

In the present report, we evaluated the potential of US and NBs as a physical method of gene transfer in cancer gene therapy using the HSV*tk*/GCV system as a therapeutic agent.

MATERIALS AND METHODS

Nano/microbubbles

Two types of NBs, Optison™ (Amersham Health PLC, Oslo, Norway) and lipid-micelle bubbles were used. Both bubbles provided very similar physical chemical properties (size distribution and ζ potential). A report on the systematic comparison of the two reagents is currently in preparation. Optison is an octafluoropropane (C_3F_8)-filled albumin microspheres that has a mean diameter between 3.0 and 4.5 μm (max. 32.0 μm). In this study, the mean concentration was set to the arithmetic average of 6.5×10^8 bubbles/mL. Lipid-micelle bubbles were created in an aqueous dispersion of 2 mg/mL 1,2-distearoyl-sn-glycero-3-phosphocholine (DSPC) (Avanti Polar Lipids, Alabaster, AL, USA) and 1 mg/mL polyethleneglycol-40 stearate (PEG) (Sigma-Aldrich Co., St. Louis, MO, USA) using a 20-kHz sonicator (Vibra Cell, Sonics & Materials, Inc., Danbury, CT, USA) in the presence of C_3F_8 gas (Aoi et al. 2006). The theoretically calculated concentration was 1.6×10^{10} bubbles/mL. The lipid bubble surface that comprised lipid molecules was confirmed by staining lipid molecules with 3 μM FM1–43 (553 nm, Abs: 570 nm, Em., Molecular Probe Inc, Eugene, OR, USA) under an inverted microscope (IX81, Olympus Co., Tokyo, Japan). The bubble size distribution was determined by using a laser diffraction particle size analyzer (particle range of 0.6 nm–7 μm, ELSZ-2, Otsuka Electronics Co. Ltd, Osaka, Japan). The peak diameters expressed in terms of the size distribution of Optison and lipid bubbles were 1689 ± 150 nm (n = 4) and 1272 ± 163 nm (n = 7), respectively. Because the volume distribution is proportional to the third power of the size, the peak of the size distribution tends to be measured as a smaller value than that of the volume distribution. The ζ potential of the bubbles was measured by the ELSZ-2 in phosphate-buffered saline without Mg_{2+} and Ca_{2+} (PBS). Zeta potential refers to the electrostatic potential generated by the accumulation of ions at the surface of a bubble that is organized into an electrical double layer. The ζ potential of the Optison and lipid bubble, was –36.9 ± 2.70 mV (n = 3) and –4.11 ± 0.74 mV (n = 4), respectively, indicating that Optison have larger mutual impulsive forces and higher stability compared with the lipid bubbles. In our previous experiments, there were no significant differences in *in-vitro* gene activity between Optison and lipid micelle bubbles (data not shown). In the following experiments, lipid-micelle bubbles and Optison were used for *in-vitro* and *in-vivo* experiments, respectively.

Cell preparation

Human lung carcinoma (A549) and murine colon carcinoma (colon26, which was abbreviated as C26 in the text) were obtained from the Cell Resource Center for Biomedical Research, Institute of Development, Aging and Cancer, Tohoku University, Sendai, Japan. Murine breast carcinoma (EMT6) cells were obtained from the American Type Culture Collection (Manassas, VA, USA). Murine breast carcinoma cells (EMT6-luc) stably expressing the firefly luciferase gene were prepared by transfected pEGFPLuc (BD Biosciences, Franklin Lakes, NJ, USA) and Lipofectin Transfer Reagent (Invitrogen, Carlsbad, CA, USA). Human colon carcinoma cells (HT29) were obtained from Cancer Research UK (London, UK), and human colon carcinoma cells (HT29-luc) stably expressing the firefly luciferase gene were obtained from Xenogen (Alameda, CA, USA). A549, C26, HT29 and HT29-luc cells were cultured under standard conditions in RPMI 1640 supplemented with 10% heat-inactivated fetal bovine serum (FBS) (Invitrogen) and 1% L-glutamine-penicillin-streptomycin (Sigma-Aldrich, St. Louis, MO, USA), whereas EMT6 cells and EMT6-luc were cultured in DMEM (Sigma-Aldrich) medium with the same supplements. Cells cultured in a 10-cm culture dish were maintained in a humidified incubator at 37° C under an atmosphere of 5% CO_2 and 95% air.

Plasmids

The luciferase reporter vector pGL3-control (Promega, Madison, WI, USA), which expresses luciferase from SV40 promoter, pGV24 vector in which HSV*tk* expression is driven by the ERBB2 promoter (Vassaux et al. 1999) and pRS303 that does not have any transgene expressed, were used as mock plasmid. pGV24 and pRS303 were referred to as pHSV*tk* and pMock, respectively.

Ultrasound

Two 1-MHz submersible US probes (Fuji Ceramics Co., Fujinomiya, Japan), 12 and 38 mm in diameter, were used for *in-vitro* and *in-vivo* experiments, respectively. Each probe was located in a test chamber (380 × 250 × 130 mm^3) filled with tap water. Each frequency was generated by a multifunction synthesizer (WF1946A; NF Co., Yokohama, Japan), amplified with a high-speed bipolar amplifier (HSA4101; NF Co.). The pressure values were measured by a PVDF needle-hydrophone (PVDF-Z44–1000; Specialty Engineering Associates, Soquel, CA, USA) at a stand-off distance of 1 mm from the transducer surface using a stage control system (Mark-204-MS, Sigma Koki, Tokyo, Japan). The signals from both the amplifier and the hydrophone were recorded into a digital phosphor oscilloscope (Wave Surfer 454, 500 MHz, 1 mol/LΩ (16 pF), LeCroy Co., Chestnut, NY, USA).

In-vitro *transfection by ultrasound and nanobubbles*

In-vitro studies were performed in accordance with the Tohoku University ethical guidelines. A549 (1 × 10^4 cells/well), HT29 (1 × 10^4 cells/well), C26 (2 × 10^4 cells/well) and EMT6 (2 × 10^4 cells/well) cells were seeded in 24-well plates in complete media at 37° C in a 5% CO_2 incubator. The next day, the medium was replaced with fresh media (200 μL), containing pMock (4 μg/mL) or pHSV*tk* (4 μg/mL) with and without NBs (10% v/v). The 24-well plates were located just above the US probe in a test chamber filled with tap water and exposed to the optimized US (intensity: 1.3 W/cm^2, duty ratio: 50%, number of pulse: 2000, exposure time: 10s). The surface of the media was disturbed by US, thus we ignored the effect of standing waves on gene expression. Because cells were seeded into wells alternately, neighboring wells were not exposed to ultrasound at the same time. The plates were incubated for 1 h at 37° C in a 5% CO_2 incubator, supplemented with 800 μL of complete media and then incubated for another 24 h at 37° C in a 5% CO_2 incubator.

In-vitro *sensitivity to GCV assays*

Twenty-four hours after transfection, the media was replaced with complete media (1 mL) containing GCV (0.1–1000 μg/mL, molecular weight 255.2; F. Hoffman-La Roche Ltd., Basel, Switzerland). The plates were incubated for another three to five days at 37° C in a 5% CO_2 incubator. Survival fractions were measured by MTT assay (Kodama et al. 2003; Martinico et al. 2006). Each experiment consisted of six to 15 samples receiving US + NB + GCV with HSV*tk* (or Mock) and six to 15 control samples receiving US and NB. For each experiment, the mean % of treated samples was divided by the mean % of control samples to give a survival fraction. The mean of six to 15 survival fractions was calculated for each condition. The survival fraction of each cell line was measured at the GCV concentration where the highest statistical significant was obtained.

RT-PCR

The total RNAs were reverse-transcribed using the RNA PCR Kit (AMV) (Takara Bio Inc., Tokyo, Japan) according to the manufacturer's instructions (1 μg of total RNA was used). The cDNAs obtained were then subjected to polymerase chain reaction (PCR) amplification (3 min at 94 °C, and 35 cycles of denaturation 95 °C for 60 s, annealing 58.4 °C for 60 s and extension 72 °C for 60 s, followed by 5 min of extension 72 °C) with either HSV*tk*-specific primers (5′-AACAATGGGCATGCCTTATGC-3′; 5′-TTATACAGGTCGCCGTTGGGG-3′, with an expected PCR product of 540 bp) or β-actin–specific primers (5′-CTGTCTGGCGGCACCACCAT-3′; 5′-GCAACTAAGTCATAGTCCGC-3′, with an expected PCR product of 254 bp). The PCR products were then separated on a 2% agarose gel.

Apoptotic assay

Apoptotic cells were detected by fluorescence microscopy (DAPI staining) and TUNEL assay. For DAPI staining, cells incubated in the presence of GCV (10 μg/mL) for 24 h after the treatment of US+NB+ HSV*tk* were stained with DAPI solution (100 ng/mL). For TUNEL assay, cells were harvested at 48 h after treatment, fixed in 4% (w/v) paraformaldehyde with PBS and then washed with PBS and stored in 70% ethanol at –20° C for at least 30 min. The ethanol solution was subsequently removed after centrifugation, and cells were treated with the enzyme terminal deoxynucleotidyl transferase and FITC-labeled dUTP using the Mebstain apoptosis kit from MBL (Nagoya, Japan) according to the manufacturer's protocol. FITC-labeled cells were measured by flow cytometry (FACSCalibur, Becton Dickinson, San Jose, CA, USA). A total of 10,000 events per sample were collected in list mode, and data were analyzed with Cell Quest software (Becton Dickinson). Fluorescence data were collected by using 488-nm excitation from a 15-mW air-cooled argon-ion laser. The emission was collected through a 530 ± 30-nm band-pass

filter (FL1-H). In addition, forward-light scatter (FSC-H) and side-light scatter (SSC-H) data were collected for each sample. The mean fluorescence uptake was defined as the number of the events multiplied by the geometric mean of the channel number.

Monitoring gene transfer in vivo

Tumors were induced by subcutaneous injection of 1×10^6 of either EMT6 or C26 cells in 6 week-old BALB/c mice (two mice for each cell line, two tumors/mouse). Ten-microgram DNA (1 μg/μL) of pGL3-control with NBs (15 μL) and saline (5 μL) were injected intratumorly for a total volume of 30 μL (day 0). The tumor was immersed into water and exposed to US at 3.0 W/cm^2 for 60 s. At day 1 and day 2, mice were anesthetized with isoflurane, subsequently received i.p. injection with luciferin (150 μg/g body weight) and were placed on the *in-vivo* imaging system. The bioluminescence signals were monitored using an IVIS100 (Xenogen Corp., Alameda, CA, USA).

Bioluminescence intensity and tumor volume

In-vivo studies were performed in accordance with the Tohoku University ethical guidelines. In this study,

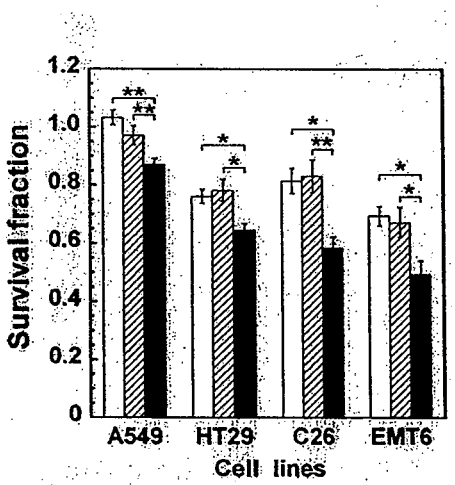

Fig. 1. Effect of NBs and US on GCV cytotoxicity in HSV*tk*-expressing cancer cells. Survival fractions were measured by MTT assay. Table 1 shows the number of samples used in Fig. 1. Each experiment consisted of six to 15 samples receiving US + NB + GCV with HSV*tk* (or Mock) and six to 15 control samples receiving US and NB. For each experiment, the mean % of treated samples was divided by the mean % of control samples to give a survival fraction. The mean of six to 15 survival fractions was calculated for each condition. □: US + NB + GCV; ▨: Mock + US + NB + GCV, ■: HSV*tk* + US + NB + GCV. A549 at day five with 5 μg/mL GCV, HT29 at day four with 10 μg/mL GCV, C26 examined at day three with 100 μg/mL GCV and EMT6 at day three with GCV 100 μg/mL). Ultrasound intensity was 1.3 W/cm^2. NB: lipid-micelle bubble. Bars represent the mean ± SEM. $*p < 0.05$; $**p < 0.01$.

Table 1. Number of samples per condition in Fig. 1.

	Control	□	▨	■
A549	6	6	6	6
HT29	6	6	6	6
C26	15	14	15	9
EMT6	12	10	9	12

A549: human lung adenocarcinoma cell, HT29; human colon carcinoma cell, C26: murine colon carcinoma cell, EMT6: murine mammary carcinoma cell. US: ultrasound, NB: nano/microbubbles, GCV: ganciclovir, Mock: pRS303 that does not have any transgene expressed, HSV*tk*: pGV24 vector in which the herpes simplex thymidine kinase (HSV*tk*) gene expression is driven by the ERBB2 promoter. □: US + NB + GCV, ▨: Mock + US + NB + GCV, ■: HSV*tk* + US + NB + GCV.

11 BALB/c mice (8- to 10-week-old) were used. Tumors were induced by subcutaneous injection of 0.25×10^6/100 μL/site to 1×10^6/100 μL/site of EMT6-luc cells into both flanks (two tumors/mouse). The intensity and volume were measured from two to 23 days after inoculation. Each mouse was anesthetized with isoflurane and subsequently received i.p. injection with luciferin (150 μg/g body weight), and placed on the *in-vivo* imaging system to measure the bioluminescence signals. The tumor volume was measured with a caliper and calculated according to the formula $(\pi/6) \times (\text{width})^2 \times (\text{length})$.

Therapeutic effect in vivo

Two types of experiments were conduced for low- and high-invasion tumors. Low-invasion case (subcutaneous tumor): SCID mice received subcutaneous injec-

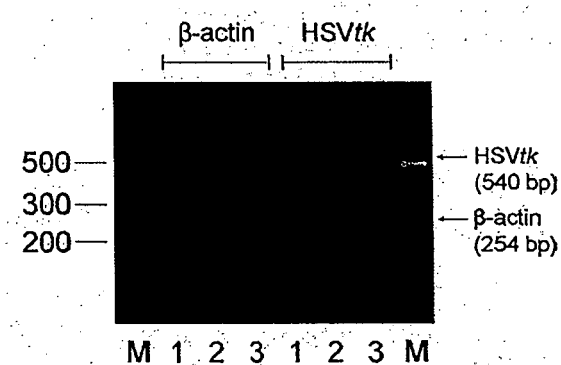

Fig. 2. Gel electrophoretic analysis of a RT-PCR reaction of HSV*tk* gene expressed in A549 cells induced by NBs and US. NB: lipid-micelle bubble. Lane M: 100-bp size ladder. Lane 1: cell alone. Lane 2: Mock + US + NB. Lane 3: HSV*tk* + US + NB. Total RNA was extracted from the cultures (pool of 6 wells) at 24 h after transfection, reverse-transcribed and amplified. The HSV*tk*-amplified fragment is 540 bp. The housekeeping gene, β-actin was 254 kb. This is a representative example from two separate experiments.

tions of 1×10^6/100 μL/site HT29-luc cells on each flank site on day 0 (2 tumors/mouse; 2 mice for control and mock groups, 3 mice for HSV*tk* group). The injection site was detectable more than three days after the injection because the skin color was changed. In addition, the site was given an India ink tattoo temporally. On days three, six, and nine, a total volume of 30 μL including 10 μL pHSV*tk* (1 μg/μg) (or pMock (1 μg/μg)) with 15 μL of NBs and 5 μL of saline was injected into the tumor site and the tumor was sonicated at 3.0 W/cm^2 for 60 s (2 tumors/mouse, 2 mice). On the same days, mice were imaged with the IVIS imaging system. From day four, GCV was administered i.p. to each mouse every day. High-invasion case (intramuscular tumor): 17 SCID mice received i.m. injection of 5×10^5/30 μL/site HT29-luc cells in each tibialis anterior muscle on day 0.

Every three days after day two, pHSV*tk* was injected into the tumor with US/NB method and GCV was injected i.p. five times per week for four weeks after day three. Eight control mice (3 mice [1 tumor/mouse] and 5 mice [2 tumors/mouse]) and three mice (1 tumor/mouse from HSV*tk* group) were culled on day 10 and the remaining six mice (3 mice in each group) were culled on day 30. On day 10, one or two tumors per each control mouse and one tumor for all mice in the treatment group were homogenized. On day 30, one tumor per mouse for all mice (3 mice in each group) was homogenized. All homogenized tumor samples were used to measure luciferase activity biochemically using a luciferase assay kit (Promega). Protein content was calculated using albumin standard curves (BCA Protein Assay Kit, Pierce, Rockford, IL, USA). Luciferase activity was converted to RLU/mg protein. Increase in the tissue temperature because of attenuation of US was ignored because the US frequency was 1 MHz and the depth of solid tumors (skin and muscle tumors) from the skin was <5 mm.

Statistical analysis

All measurements are expressed as mean ± SEM (standard error of mean). An overall difference between the groups was determined by one-way analysis of variance (ANOVA). Comparisons between two samples were made using Student's *t*-test. When the one-way

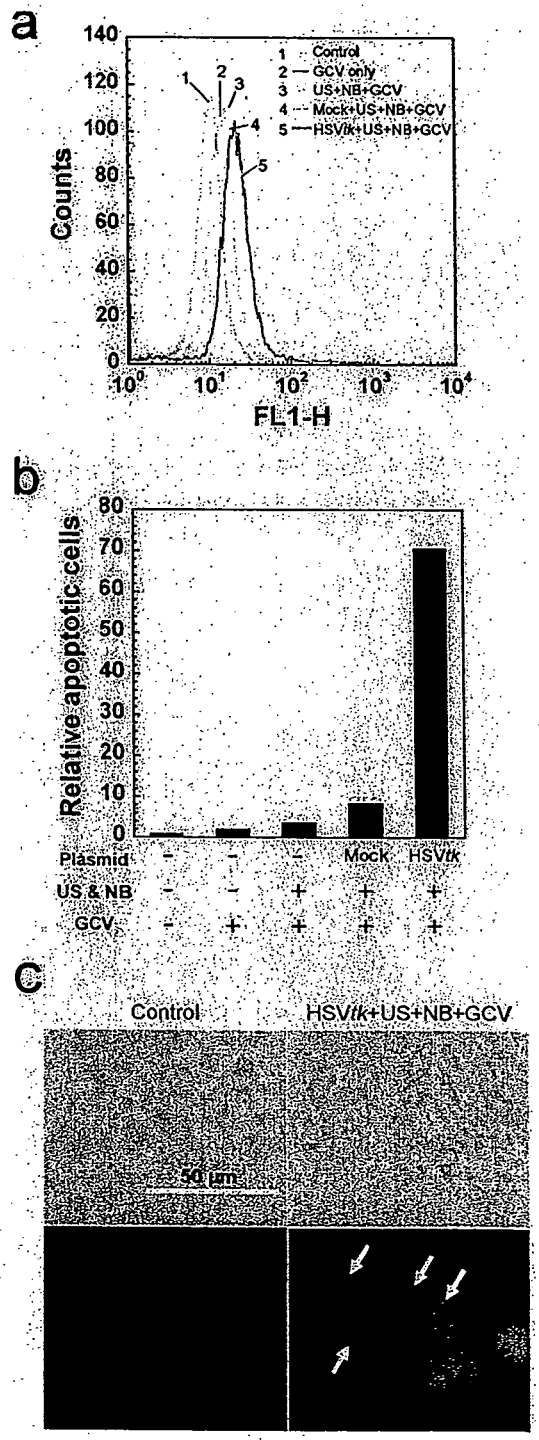

Fig. 3. Apoptosis analysis. (a) Histogram shows DNA fragmentation by TUNEL assay in A549 cells, measured at 48 h after the GCV treatment. GCV was 10 μg/mL. 1: Control (cell alone); 2: GCV alone; 3: US + NB + GCV; 4: Mock + US + NB + GCV; 5: HSV*tk* + US + NB + GCV. Cells were shifted to the higher fluorescence intensity values with increasing the number. (b) Number of TUNEL-positive cells obtained in Fig. 3a, expressed in bar chart. The emission was collected through a 530 ± 30-nm band-pass filter (FL1-H). The mean fluorescence uptake was defined as the number of the events multiplied by the geometric mean of the channel number, which was normalized with that of control cells alone. (c) Apoptosis in A549 cells was investigated by DAPI staining morphologically. A549 cells was incubated in the presence of GCV (10 μg/mL) for 24 h after the treatment of US + NB + HSV*tk*. NB: lipid-micelle bubble.

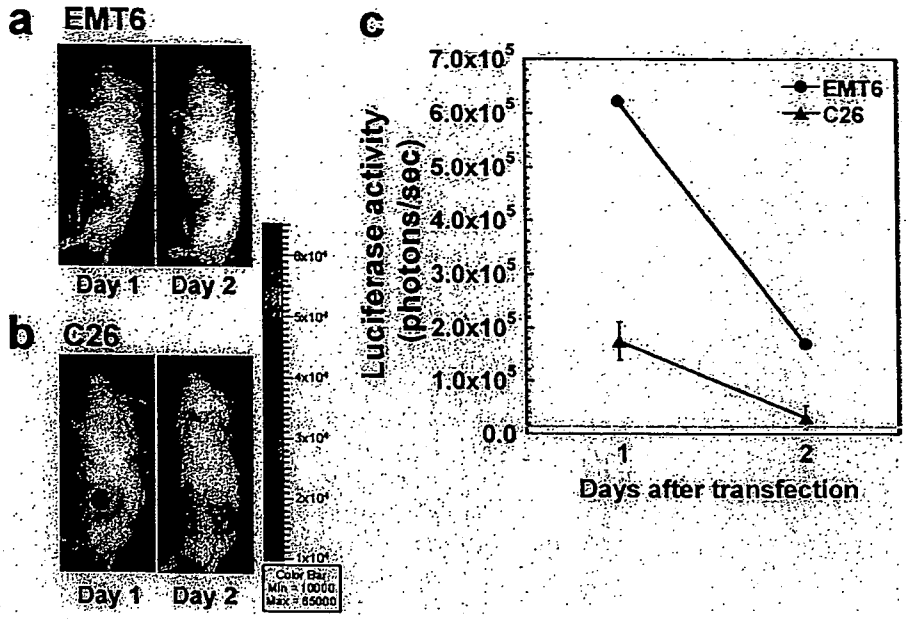

Fig. 4. Kinetics of luciferase gene expression in tumor-bearing BALB/c mice after gene transfection with US and NB. Two cell lines, EMT6 and C26, were used. Each cell line was injected into both flanks per mouse. Two mice were used for each cell line. (a, b) Representative images showing luciferase gene expression in the tumor of each cell on days 1 and 2. Color bar units represent photons/s/cm^2. (a) EMT6 cells. Gene expression was detected in only one flank. (b) C26 cells. Gene expression was detected in three flanks. (c) Luciferase activity with elapsed time. Background level (1.46×10^4 photons/s). Gene expression vanished in two days after the transfection by the US/NB method. Ultrasound intensity was 3.0 W/cm^2. NB: Optison. Bars represent the mean ± SEM.

ANOVA was significant and there were three samples, the differences between each group were estimated using the Tukey-Kramer test. The differences were considered to be significant at $p < 0.05$.

RESULTS

Gene transfer and GCV-mediated cytotoxicity in vitro

We first demonstrated that the combination of NBs with US could induce the sensitivity of different cell lines (A549, HT29, C26, EMT6) to killing by GCV *in vitro*. Because the sensitivity to GCV depends on the type of cells, the concentration of GCV and the assay day of cytotoxicity were varied for each cell line. MTT assay showed that exposure of US alone to cells (without NBs) did not induce cell damage (>0.95) (data not shown). Therefore, we compared HSV*tk* + US + NB + GCV with US +NB + GCV and Mock + US +NB + GCV. The MTT assay of four cell lines shows the significant cytotoxicity to GCV with HSV*tk* + US + NB + GCV compared with the control groups (Fig. 1). The sample numbers for each condition were shown in Table 1. HSV*tk* gene transfer was confirmed by RT-PCR (Fig. 2), where samples obtained under the same condition of Fig. 1 were analyzed. HSV*tk* + US + NB shows the single clear fragment (540 bp) compared with cell alone and Mock + US + NB, whereas the fragment (254 bp) of β-actin was observed for each condition.

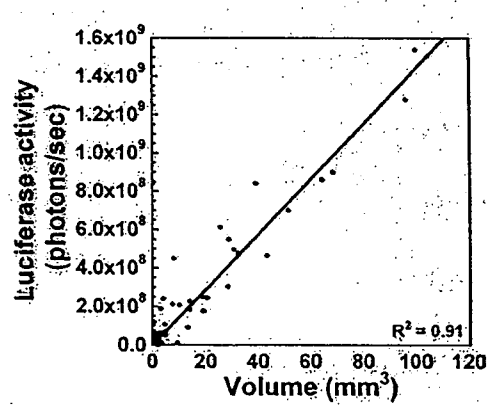

Fig. 5. The relationship between the light intensity and solid volume of EMT6-luc cells stably expressing the firefly luciferase gene. Cells were injected subcutaneously in mouse flanks (2 tumors/mouse). The number of mice and tumors was seven and 11, respectively. The intensity was measured from two to 23 days after inoculation. The volume was measured with a caliper. Tumor volume was calculated according to the formula $(\pi/6) \times (\text{width})^2 \times (\text{length})$.

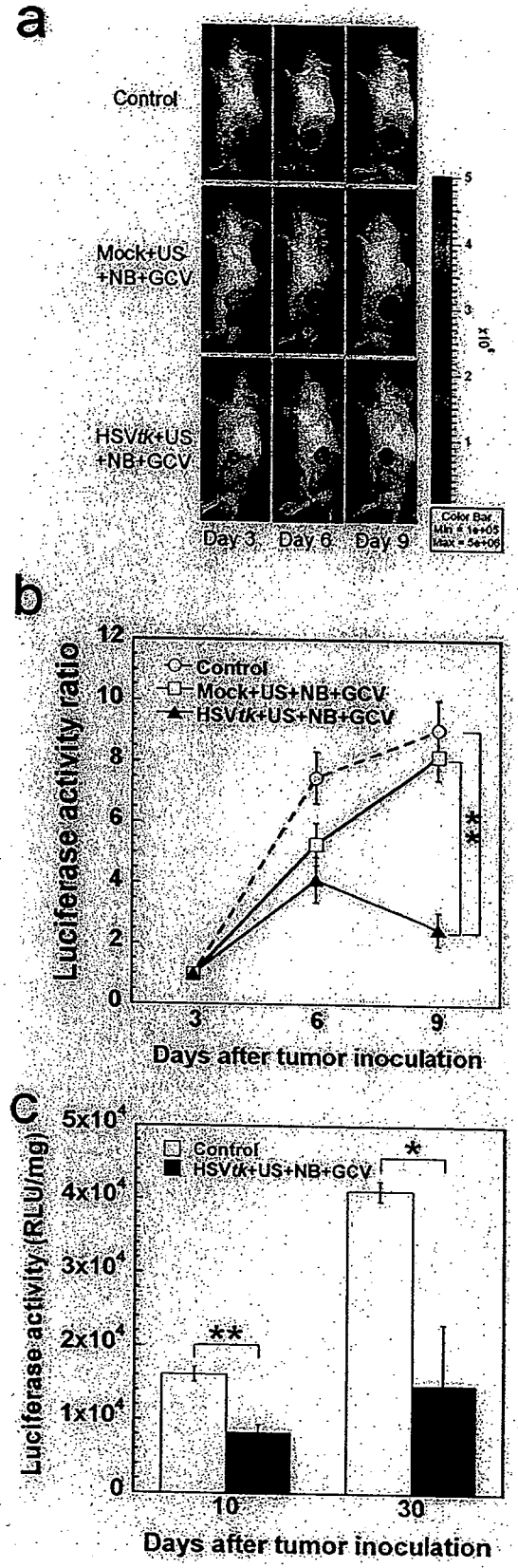

Apoptosis

We investigated whether the cytotoxicity was induced *via* apoptosis. Flow cytometry analysis of the TUNEL assay for A549 cells shows the curve in HSV*tk* + US + NB + GCV shifts largely to the right compared with other control groups, suggesting that dUTP labeled with biotin binds to DNA strand break (Fig. 3a). Figure 3b shows the histogram of Fig. 3a, indicating that the uptake of dUTP for HSV*tk* + US + NB + GCV is enhanced by a factor of 7 compared with Mock + US + NB + GCV. Because dUTP is also incorporated into DNA strands of necrotic cells, we stained A549 cells with DAPI staining and investigated the induction of apoptosis in the cells morphologically (Fig. 3c). As seen in Fig. 3c, apoptotic characteristics such as plasma membrane convolution, cytoplasmic blebbing, and nuclear condensation and fragmentation are observed; thus apoptosis is induced by the effect of HSV*tk*/GCV with the US/NB method.

Gene transfer in vivo*: Marker study*

The US/NB method induces a transient gene expression. First we investigated the kinetics of gene expression in tumor-bearing BALB/c mice by the US/NB method and determined the administration times by the US + NB. Two cell lines, EMT6 (Fig. 4a) and C26 (Fig. 4b), were used. Luciferase gene expression in these different solid tumors showed the same kinetics. The maximum luciferase activity was obtained at day one after transfection and reduced to the background level at day two (Fig. 4c). From these results, we delivered pHSV*tk* into tumor-bearing SCID mice by the US/NB method two to three times per week to maintain a high HSV*tk* gene expression level.

Fig. 6. Effect of GCV upon intratumoral HSV*tk* gene transfer with ultrasound and NB. (a, b) Data obtained with HT29-luc cells (1×10^6/100 μL of saline) injected subcutaneously into SCID mice. (a) Representative images showing bioluminescence in the tumors of each group on days three, six and nine. Color bar units represent photons/s/cm^2. (b) Bioluminescence was quantified at days three, six and nine. Statistical analysis was performed with the Tukey-Kramer test. Ultrasound intensity was 3.0 W/cm^2. NB: Optison. Bars represent the mean ± SEM; $^{**}p < 0.01$. (c) Tumors were induced by i.m. injection of HT29-luc cells (5×10^5/30 μL of saline) into each tibialis anterior muscle of SCID mice for each group on day zero, and from day three, GCV 40 (mg/kg) diluted in PBS was given daily. Tumors were removed and homogenized at 10 and 30 d. The luciferase activity was measured with a luminometer. Statistical analysis was performed by using Student's *t*-test. Ultrasound intensity was 3.0 W/cm^2. NB: Optison. Bars represent the mean ± SEM; $^{*}p < 0.05$, $^{**}p < 0.01$.

Bioluminescence intensity and tumor volume

We investigated the linearity between the bioluminescence intensity and the solid tumor volume. EMT6-luc cells were injected subcutaneously. The cells allowed us to measure the size of the tumor because the cells are relatively low invasive and the boundary of the generated solid tumor is identified relatively easily. The volume was measured with a caliper and the light intensity was obtained with the *in-vivo* imaging system. As seen in Fig. 5, the linearity between the bioluminescence intensity and the tumor volume was kept up to 100 mm^3 (the width of solid tumor was <6 mm). Therefore, tumors with a volume <100 mm^3 were analyzed with the *in-vivo* imaging system in the experiment.

Therapeutic effects in vivo

Based on Figs. 4 and 5, we investigated the antitumor effect of US/NB-mediated HSV*tk* gene transfer to HT29-luc bearing SCID mice for the first experiment. The cells were injected and grown subcutaneously. The tumors were transduced three days after tumor cell inoculation and gene transfer was repeated on days six and nine. Daily i.p. injection of GCV (40 mg/kg) was administered from day four. Figure 6a and b show that a very significant reduction in tumor volume in mice treated with HSV*tk*, US, NB and GCV compared with control groups indicate that the US/NB method has therapeutic effects.

In clinical practice, most tumors may not be distinguished clearly from normal tissue as they are infiltrated into normal tissue. In a second experiment, HT29-luc cells were injected into the TA muscle and the tumors treated by US/NB-mediated gene transfer and GCV. US/NB-mediated HSV*tk* gene transfer was performed every three days from day four and GCV (40 mg/kg) was administered five times per week. Bioluminescence of the tumors *in vivo*, as well as enzymatic activity on biopsies, was measured (Fig. 6c). Luciferase activity measured biochemically on day 10 shows a statistical difference in tumor burden between control and HSV*tk* + US + NB + GCV. Furthermore, there was a statistical difference in tumor burden on day 30, with mice treated with HSV*tk* + US + NB + GCV, showing a 4 times reduction in tumor burden compared with control (Fig. 6c). During the course of these experiments, no weight reduction was observed in treated and untreated mice. Altogether, these results demonstrate the potential of HSV*tk* + US + NB + GCV treatment.

DISCUSSION

The concept of the molecular delivery method using US and NB is to induce a transient membrane permeability of cells, followed by the entry of exogenous molecules into the cells. It has been suggested that the impulsive pressures generated by either the collapse of NBs or cavitation bubbles created by the collapse of NBs are able to induce a transient permeabilization of cells, followed by the entry of exogenous molecules into cells. Gene or oligodeoxynucleotide transfer using NB and US has already been reported (Kodama et al. 2005, 2006a, 2006b; Takahashi et al. 2007), but in this manuscript we demonstrate that this technology can be applied successfully to cancer gene therapy. *In-vitro* US/NB-mediated transfer of the HSV*tk* gene (Fig. 2) and incubation of the transduced cells with GCV leads to reduced cell survival (Fig. 1). This DNA-dependent cell kill was achieved through apoptosis (Fig. 3), as expected from the well-established mode of action of HSV*tk*/GCV (Freeman et al. 1993; Hamel et al. 1996; Wallace et al. 1996; Yoon et al. 1999).

In the present *in-vivo* study, we evaluated the *in-vivo* cytotoxicity by US/NB-mediated gene transfer by bioluminescence. The linearity between the intensity of bioluminescence and the tumor volume was kept up to a volume of 100 mm^3 (the width was <6 mm) (Fig. 5), where tumor volume was calculated according to the formula $(\pi/6) \times (\text{width})^2 \times (\text{length})$. In general, tumor size correlates closely with light intensity (Mendel et al. 2003; Soling et al. 2004). In agreement with our observations, Soling et al. (2004) reported that tumor size is not correlated with light intensity when the tumor becomes large (>12–15 mm in diameter) based on the same equation. In fact, in our recent studies, we have found that bioluminescence measurement collected using the IVIS imaging system showed a great correlation between mean bioluminescence and mean 3D tumor volume quantified using high frequency ultrasound imaging system (data not shown).

In-vivo gene expression was detectable 24 h after transfection and was dramatically reduced 48 h later (Fig. 4), highlighting the transient nature of US/NB-mediated gene transfer. This kinetics is in sharp contrast with adenovirus-mediated (Groot-Wassink et al. 2002, 2004) or nonviral gene transfer (Harada-Shiba et al. 2002; Yoshino et al. 2006), which usually lead to a maximal level of expression 48 h after transduction and can last several days at least. The transient nature of US/NB-mediated gene delivery has implications when applied in the context of pro-drug activation therapy: gene delivery must be repeated and the pro-drug must be provided shortly after transduction. This transient expression is likely to be the result of rapid plasmid DNA degradation.

In many *in-vivo* experiments, solid tumors are induced subcutaneously and used as therapeutic targets. However, therapeutic effects need to be considered using tumors infiltrated into normal tissues. In the present

experiment, we provided data demonstrating therapeutic effects of US/NB-mediated gene transfer for two types of tumors. One was subcutaneous (low-invasive) and the other was i.m. tumors (high-invasive). Figure 6 clearly shows the efficacy of the treatment with low-invasive and (Fig. 6a and b) high-invasive tumors (Fig. 6c) by US/NB-mediated gene transfer.

Considering the efficacy of the current version of NBs presented in this report and the potential for chemical modifications of the shell material (Li et al. 2003; Wang et al. 2005), and for incorporation of specific ligands in the shell membrane to enhance the tissue-specificity against the target site (Lindner 2004), the system associating NB, DNA and US could provide an alternative option to viral cancer gene therapy.

Acknowledgments—We thank Kiyoe Konno and Sachiko Horie for technical assistance. This work was supported in part by the Encouraging Development of Strategic Research Center, Special Coordination Funds for Promoting Science and Technology, MEXT (Ministry of Education, Culture, Sports, Science and Technology). T.K. acknowledges Grant-in-Aid for Scientific Research (B) (17300168), Grants-in-Aid for Exploratory Research (18650140), Grant-in-Aid for Scientific Research on Priority Area, MEXT (17012002, 18014002) and Research on Advanced Medical Technology, The Ministry of Health Labour and Welfare (H17-nano-006 and H19-nano-010). G.V. acknowledges program and projects grants from Cancer Research UK, and INSERM and Institut National du Cancer (INCa). GCV was donated from F. Hoffman-La Roche Ltd., Basel, Switzerland.

REFERENCES

Ammi AY, Cleveland RO, Mamou J, Wang GI, Bridal SL, O'Brien WD. Ultrasonic contrast agent shell rupture detected by inertial cavitation and rebound signals. IEEE Trans Ultrason Ferroelectr Freq Control 2006;53:126–136.

Aoi A, Konno K, Shinohara F, Mori S, Vassaux G, Kodama T. Effects of anti-cancer drug of cisplatin using nanobubbles and ultrasound. Ultrasound Med Biol 2006;32:280.

Chen SH, Chen XH, Wang Y, Kosai K, Finegold MJ, Rich SS, Woo SL. Combination gene therapy for liver metastasis of colon carcinoma *in vivo*. Proc Natl Acad Sci U S A 1995;92:2577–2581.

Chomas JE, Dayton P, Allen J, Morgan K, Ferrara KW. Mechanisms of contrast agent destruction. IEEE Trans Ultrason Ferroelectr Freq Control 2001;48:232–248.

Fillat C, Carrio M, Cascante A, Sangro B. Suicide gene therapy mediated by the Herpes Simplex virus thymidine kinase gene/Ganciclovir system: Fifteen years of application. Curr Gene Ther 2003;3:13–26.

Freeman SM, Abboud CN, Whartenby KA, Packman CH, Koeplin DS, Moolten FL, Abraham GN. The "bystander effect": Tumor regression when a fraction of the tumor mass is genetically modified. Cancer Res 1993;53:5274–5283.

Groot-Wassink T, Aboagye EO, Glaser M, Lemoine NR, Vassaux G. Adenovirus biodistribution and noninvasive imaging of gene expression *in vivo* by positron emission tomography using human sodium/iodide symporter as reporter gene. Hum Gene Ther 2002; 13:1723–1735.

Groot-Wassink T, Aboagye EO, Wang Y, Lemoine NR, Keith WN, Vassaux G. Noninvasive imaging of the transcriptional activities of human telomerase promoter fragments in mice. Cancer Res 2004; 64:4906–4911.

Hamel W, Magnelli L, Chiarugi VP, Israel MA. Herpes simplex virus thymidine kinase/ganciclovir-mediated apoptotic death of bystander cells. Cancer Res 1996;56:2697–2702.

Harada-Shiba M, Yamauchi K, Harada A, Takamisawa I, Shimokado K, Kataoka K. Polyion complex micelles as vectors in gene therapy—Pharmacokinetics and *in vivo* gene transfer. Gene Ther 2002; 9:407–414.

Harvey CJ, Blomley MJ, Eckersley RJ, Cosgrove DO. Developments in ultrasound contrast media. Eur Radiol 2001;11:675–689.

Keller PM, Fyfe JA, Beauchamp L, Lubbers CM, Furman PA, Schaeffer HJ, Elion GB. Enzymatic phosphorylation of acyclic nucleoside analogs and correlations with antiherpetic activities. Biochem Pharmacol 1981;30:3071–3077.

Kodama T, Aoi A, Vassaux G, Mori S, Morikawa H, Koshiyama K, Yano T, Fujikawa S, Tomita Y. A non-invasive tissue-specific molecular delivery method of cancer gene therapy. Minim Invasive Ther Allied Technol 2006a;15:226–229.

Kodama T, Doukas AG, Hamblin MR. Delivery of ribosome-inactivating protein toxin into cancer cells with shock waves. Cancer Lett 2003;189:69–75.

Kodama T, Tan PH, Offiah I, Partridge T, Cook T, George AJ, Blomley MJ. Delivery of oligodeoxynucleotides into human saphenous veins and the adjunct effect of ultrasound and microbubbles. Ultrasound Med Biol 2005;31:1683–1691.

Kodama T, Tomita Y, Koshiyama K, Blomley MJ. Transfection effect of microbubbles on cells in superposed ultrasound waves and behavior of cavitation bubble. Ultrasound Med Biol 2006b;32: 905–914.

Li T, Tachibana K, Kuroki M, Kuroki M. Gene transfer with echo-enhanced contrast agents: Comparison between Albunex, Optison, and Levovist in mice—Initial results. Radiology 2003;229:423–428.

Lindner JR. Microbubbles in medical imaging: current applications and future directions. Nat Rev Drug Discov 2004;3:527–532.

Martinico SC, Jezzard S, Sturt NJ, Michils G, Tejpar S, Phillips RK, Vassaux G. Assessment of endostatin gene therapy for familial adenomatous polyposis-related desmoid tumors. Cancer Res 2006; 66:8233–8240.

McCulloch M, Gresser C, Moos S, Odabashian J, Jasper S, Bednarz J, Burgess P, Carney D, Moore V, Sisk E, Waggoner A, Witt S, Adams D. l. Ultrasound contrast physics: A series on contrast echocardiography, article 3. J Am Soc Echocardiogr 2000;13:959–967.

Mendel DB, Laird AD, Xin X, Louie SG, Christensen JG, Li G, Schreck RE, Abrams TJ, Ngai TJ, Lee LB, Murray LJ, Carver J, Chan E, Moss KG, Haznedar JO, Sukbuntherng J, Blake RA, Sun L, Tang C, Miller T, Shirazian S, McMahon G, Cherrington JM. In vivo antitumor activity of SU11248, a novel tyrosine kinase inhibitor targeting vascular endothelial growth factor and platelet-derived growth factor receptors: Determination of a pharmacokinetic/pharmacodynamic relationship. Clin Cancer Res 2003;9:327–337.

Mesnil M, Yamasaki H. Bystander effect in herpes simplex virus-thymidine kinase/ganciclovir cancer gene therapy: Role of gap-junctional intercellular communication. Cancer Res 2000;60:3989–3999.

Oliver S, Bubley G, Crumpacker C. Inhibition of HSV-transformed murine cells by nucleoside analogs, 2′-NDG and 2′-nor-cGMP: Mechanisms of inhibition and reversal by exogenous nucleosides. Virology 1985;145:84–93.

Pitt WG, Husseini GA, Staples BJ. Ultrasonic drug delivery—A general review. Expert Opin Drug Deliv 2004;1:37–56.

Soling A, Theiss C, Jungmichel S, Rainov NG. A dual function fusion protein of Herpes simplex virus type 1 thymidine kinase and firefly luciferase for noninvasive *in vivo* imaging of gene therapy in malignant glioma. Genet Vaccines Ther 2004;2:7.

Takahashi M, Kido K, Aoi A, Furukawa H, Ono M, Kodama T. Spinal gene transfer using ultrasound and microbubbles. J Control Release 2007;117:267–272.

Vassaux G, Hurst HC, Lemoine NR. Insulation of a conditionally expressed transgene in an adenoviral vector. Gene Ther 1999;6: 1192–1197.

Vassaux G, Martin-Duque P. Use of suicide genes for cancer gene therapy: Study of the different approaches. Expert Opin Biol Ther 2004;4:519–530.

Wallace H, Clarke AR, Harrison DJ, Hooper ML, Bishop JO. Ganciclovir-induced ablation non-proliferating thyrocytes expressing herpesvirus thymidine kinase occurs by p53-independent apoptosis. Oncogene 1996;13:55–61.

Wang X, Liang HD, Dong B, Lu QL, Blomley MJ. Gene transfer with microbubble ultrasound and plasmid DNA into skeletal muscle of mice: Comparison between commercially available microbubble contrast agents. Radiology 2005;237:224–229.

Wu J, Tong J. Experimental study of stability of a contrast agent in an ultrasound field. Ultrasound Med Biol 1998;24:257–265.

Yoon SS, Carroll NM, Chiocca EA, Tanabe KK. Influence of p53 on herpes simplex virus type 1 vectors for cancer gene therapy. J Gastrointest Surg 1999;3:34–48.

Yoshino H, Hashizume K, Kobayashi E. Naked plasmid DNA transfer to the porcine liver using rapid injection with large volume. Gene Ther 2006;13:1696–1702.

Available online at www.sciencedirect.com
ScienceDirect
Journal of Controlled Release 117 (2007) 267–272
journal of controlled release
www.elsevier.com/locate/jconrel
GENE DELIVERY

Spinal gene transfer using ultrasound and microbubbles

Masahiko Takahashi [a,*], Kanta Kido [a], Atsuko Aoi [a,b], Hiroshi Furukawa [c], Masao Ono [c], Tetsuya Kodama [b]

[a] Department of Oral Medicine and Surgery, Tohoku University Graduate School of Dentistry, Japan
[b] Department of Nanomedicine, Tohoku University Biomedical Engineering Research Organization, Japan
[c] Department of Pathology, Tohoku University Graduate School of Medicine, Japan

Received 19 June 2006; accepted 24 October 2006
Available online 6 November 2006

Abstract

Spinal gene therapy is a promising option for treating various spinal-related disorders. Several previous studies using viral vectors reported successful transfer of therapeutic genes into the spinal nerve system. However, because of the considerable immunogenicity related to the use of viruses, non-viral gene transfer still needs to be developed. One possible approach is the combined use of ultrasound and echo-contrast microbubbles. The present study shows that this method can be applied for targeted intrathecal gene delivery. We intrathecally injected a mixture of plasmid-DNA encoded with luciferase and commercially available albumin microbubbles by needle puncture at the lower lumbar intervertebral space in mice. Subsequent percutaneous ultrasonication on the lumbar vertebrae significantly enhanced the luciferase expression, analyzed by imaging luciferin bioluminescence, in the dorsal meningeal cells at the insonated region. No apparent neurological damages were induced by the present spinal interventions. In addition to the general benefits of the combined use of ultrasound and microbubbles, our approach can offer some advantages specific to spinal gene transfection including minimal invasiveness of simple percutaneous dural puncture, targetability due to the limited access of ultrasound waves through anatomical apertures of the vertebrae, and possible paracrine delivery of therapeutic molecules to the spinal nerve system.

Keywords: Gene therapy; Spinal disorder; Intrathecal delivery; Ultrasound; Microbubble

1. Introduction

Spinal gene transfer is expected to become a promising option for treating various spinal-related disorders including nerve injury, degenerative diseases, neoplasm, and chronic pain [1,2]. To date, the most widely used vehicles for gene delivery are viral vectors. Recent animal studies using adenovirus vectors indicated that direct spinal injection of specific growth-factor genes achieved functional recovery after acute spinal cord injury [3–5]. The feasibility of virus-mediated gene transfer to treat chronic pain has been also explored using the precursor genes of endogenous opioids [6,7]. The targeted spinal tissues for the opioid-gene transfer can be both meningeal and parenchyma cells. Among the utilized viral vectors that are mostly derived either from adenoviruses, adeno-associated viruses, herpes simplex viruses or retroviruses [8], herpes vectors may be the most promising for antinociceptive gene therapy because of its high selectivity to primary afferent neurons [2,9].

Despite such experimental successes in virus-mediated gene delivery, however, alternative non-viral transgene applications need to be developed because the clinical use of viral vectors is limited by such possible disadvantages as immunogenic properties, inflammatory responses, and the difficulty of producing large amounts of pure virus. In this context, it has been reported recently that the emission of high-pressure ultrasound in combination with echo-contrast agents, microbubbles, can facilitate gene transfection into cells [10]. Possible explanations for the mechanisms include the production of transient pores on the cell membranes as well as an increase in the

* Corresponding author. Division of Dento-oral Anesthesiology, Department of Oral Medicine and Surgery, Tohoku University Graduate School of Dentistry, 4-1 Seiryo-machi, Aoba-ku, Sendai 980-8575, Japan. Tel./fax: +81 22 717 8401.
E-mail address: m-takaha@mail.tains.tohoku.ac.jp (M. Takahashi).

0168-3659/$ - see front matter © 2006 Elsevier B.V. All rights reserved.
doi:10.1016/j.jconrel.2006.10.026

membrane fluidity by impulsive pressures raised when microbubbles are disrupted by ultrasound [11,12]. The combined use of microbubbles and ultrasound for gene delivery has several advantages including low toxicity, low immunogenicity, low invasiveness, high target selectivity, and repeatable applicability [11]. In the present study, we focused on spinal gene delivery and demonstrated that percutaneous ultrasonication in combination with intrathecal microbubbles facilitated gene transfection in spinal meningeal cells in mice.

2. Materials and methods

2.1. Animals

The study was approved by the Animal Care Committee of Tohoku University Graduate School of Medicine. Male inbred BALB/c mice were purchased from the institutional breeding facilities at 5–6 weeks of age and maintained in an antigen- and virus-free room (22±1 °C, 60±10% relative humidity, 12 h/12 h light/dark cycle, food and water *ad libitum*). The mice were studied at 7–8 weeks of age.

2.2. Plasmid DNA

pCMV-luciferase-GL3 (pcLuc-GL3: 7.4 kb) was constructed by cloning the luciferase gene from the pGL3-Control Vector (Promega Corp., Madison, WI, USA) into pcDNA3 (5.4 kb) (Invitrogen, San Diego, CA, USA) at the *Hin*dIII and *Bam*HI sites. Plasmid DNA was purified with a QIAGEN plasmid isolation kit (QIAGEN, Hilden, Germany) and prepared at a final concentration of 1 mg/ml.

2.3. Intrathecal transfection of plasmid DNA

Mice were anesthetized with an intraperitoneal injection of sodium pentobarbital (80 mg/kg) and immobilized in a prone position on an acrylic plate. Intrathecal access was accomplished by percutaneous lumbar puncture through the 4/5th or 5/6th intervertebral space using a 27-gauge stainless-steel needle according to the Hylden and Wilcox technique with modification [13]. Dural penetration of the needle was confirmed by inspecting tail flicks of the mice. A total volume of 10 μl containing 5 μg plasmid and commercially available albumin-coated octa-fluoropropane gas microbubbles (MB), Optison™ (Amersham Health, Oslo, Norway; $5–8\times10^8$/ml, 3–4.5 μm in diameter), in phosphate buffered saline at a final MB concentration either 0, 20, or 50 v/v% was then injected slowly into the intrathecal space using a 50-μl microsyringe (Hamilton, Bonaduz, GR, Switzerland). A mixture of the plasmid with MB was prepared by gentle hand shaking immediately before injection. Immediately after the intrathecal injection, the mice were placed at a vertical position in a 37 °C water bath and dorsally insonated for 1 min at the vertebral region that had been injected using an ultrasound-emitting transducer (6 mm in diameter; Fuji Ceramics Co., Fujinomiya, Japan). The ultrasound (US) parameters used were as follows: central frequency, 950 kHz; duty ratio, 20%; the average intensity per cross section, 1.3 W/cm^2; acoustic pressure at a standoff distance of 1 mm from the transducer surface, 0.6 MPa; energy, 2.4 J/cm^2. After the insonation, the mice were dried and kept under a heat lamp until recovery from anesthesia.

2.4. Analysis of luciferase activity

Mice were killed by neck dislocation under deep anesthesia with isoflurane at 1, 3, 7 days after transfection of the luciferase gene. The spinal cord was harvested *en bloc* at the level of the lower thoracic to sacral region by careful dissection of the vertebrae and placed on a dish plate. Subsequently, the tissue was fully covered with Luciferin 30 mg in 1 ml PBS (Promega Co., Madison, WI, USA). Luciferin bioluminescence was immediately quantified as the luciferase activity using an *in vivo* imaging system (IVIS™, Xenogen Co., Alameda, CA, USA) [14].

2.5. Immunohistochemistry

The harvested spinal cords were preserved in 10% PFA for 4 h and then embedded in paraffin and sectioned. Sections (4 μm thickness) were evaluated for the presence of luciferase protein by immunostaining. The sections were deparaffinized in xylene for 5 min 3×, rehydrated through graded ethanol and equilibrated in PBS. The sections were incubated in 3% H_2O_2 for 30 min to dampen endogenous peroxidase activity. They were incubated for 30 min at room temperature with 10% normal goat serum (Nichirei Biosciences Inc., Tokyo) to reduce nonspecific protein binding. After a wash in PBS, the sections were incubated with biotin-labeled rabbit anti-luciferase antibody (0.5 g/ml) (Cortex Biochem, San Leandro, CA, USA) overnight at 4 °C. The following day, after three washes in PBS, immunoreactivity was detected using an anti-rabbit IgG Histofine SAB-PO(M) kit (Nichirei Biosciences Inc., Tokyo, Japan) and diaminobenzidine (DAB) as a chromogen according to the manufacturer's protocols. After color development, the spinal cord sections were counterstained with hematoxylin and were then dehydrated, cleared, and mounted on slides.

2.6. Assessment of post-transfectional spinal injury

2.6.1. Thermal nociception

For assessing the nociceptive responses to thermal stimuli after the intrathecal procedure, the paw withdrawal latencies following exposure to infra-red radiant heat were determined [15] using a commercial device (7370-Planter Test, Ugo Basille, Comerio, Italy) three days after the gene transfection. Mice were placed in a clear plastic chamber (210 mm × 105 mm × 130 mm) with a glass floor and allowed to acclimate for at least 5 min. After the acclimation period, radiant heat was projected to the hind paw and time count was started. The heat projection was made through a 5 mm × 10 mm aperture in the top of a movable case containing the radiant heat source that was positioned under the glass floor directly beneath the paw. The radiant heat source consisted of a high intensity projecting Halogen lamp bulb (8 V–50 W) located 40 mm below the floor. The time count was stopped when the mouse withdrew its paw. Mice were tested

with three determinations each at the right and left paw and were allowed to rest for at least 30 min between each session.

2.6.2. Rotarod

For assessing motor function after the intrathecal procedure, mice were tested using a rotarod (IITC; Life Science Instrument, Woodland Hills, CA, USA) three days after the gene transfection. The rod had a diameter of 3.8 cm and was accelerated from 0 to 30 rpm over a 17.5-s period. The total time that the mice remained on the rotarod was measured. The time count was stopped when mice fell from the rod or when they rotated around completely two times without walking [16]. Mice were tested with three trials and were allowed to rest for at least 30 min between each session.

2.7. Statistical analysis

All values are expressed as mean±SEM. Statistical analysis for the spinal luciferase activities was performed by one-factor analysis of variance (ANOVA) with Fisher's protected least significant difference test (Fisher's PLSD) as a post-hoc procedure. Unpaired Student-*T* test was used for the behavioral evaluations. Statistical significance was defined as $p<0.05$.

3. Results

3.1. Effects of microbubbles and ultrasound on spinal gene transfection

Fig. 1 shows representative views of luciferin bioluminescence in the mouse spinal cord obtained by the imaging system (sum of photon counts from a region of interest at 5 min is presented). The spinal luciferase activities determined one day after four different treatments (DNA alone, DNA+MB, DNA+US, and DNA+MB+US) are shown in Fig. 2a. The concentration of MB used was 50%. The luciferase activities in the treatments with DNA+MB and DNA+US were as low as that with DNA alone. In contrast, ultrasonication after the DNA+MB injection significantly increased the luciferase activity by approximately 25 fold compared to the other treatments ($p<0.001$).

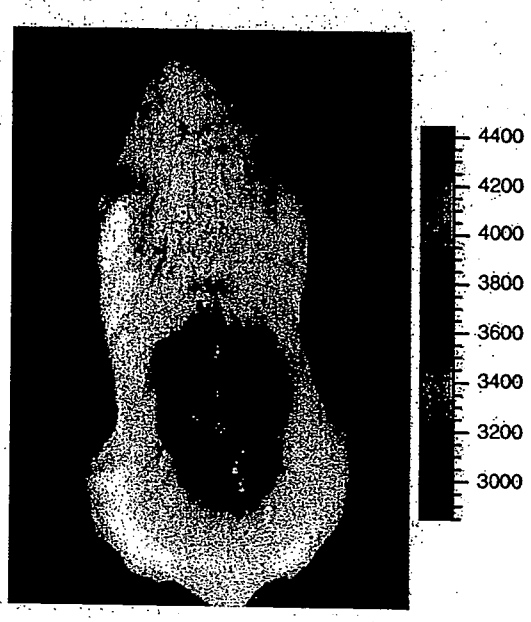

Fig. 1. Representative image showing luciferin bioluminescence (IVIS™, Xenogen Co., Alameda, CA, USA) in the spinal cord of BALB/c mice a day after the intrathecal injection of plasmid DNA and microbubbles (Optison™, Amersham Health, Oslo, Norway) followed by percutaneous ultrasonication. Imaging time is 5 min. Color bar units represent photons s^{-1} cm^{-2}.

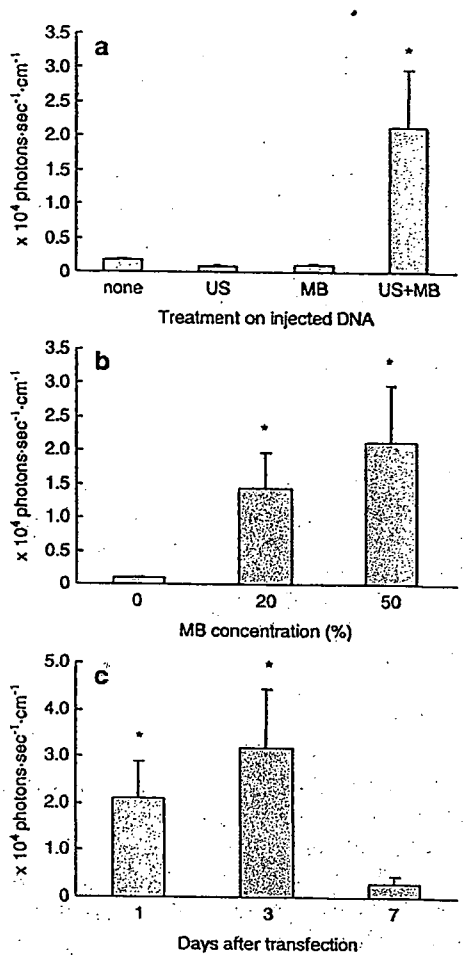

Fig. 2. Plasmid-derived spinal luciferase activity represented by luciferin bioluminescence in mice subjected to intrathecal gene delivery using ultrasound and microbubbles. The ultrasound parameters were as follows: central frequency, 950 kHz; duty ratio, 20%; the average intensity per cross section, 1.3 W/cm^2; acoustic pressure at a standoff distance of 1-mm from the transducer surface, 0.6 MPa; energy, 2.4 J/cm^2; exposure time, 1 min. (a) Treatment effects of ultrasound and 50% microbubbles one day after the application. Combined use of ultrasound and microbubbles significantly enhanced the gene transfection compared to the other treatments. (b) Effects of the microbubble concentration on the spinal gene expression. Microbubbles at concentrations of both 20 and 50% significantly enhanced the gene transfection one day after the application. No significant difference was found between the luciferase activities in mice treated with the two concentrations. (c) Time course of spinal gene expression in mice treated with ultrasound and 50% microbubbles. Luciferase activity significantly increased at 1 and 3 days after gene transfection which disappeared by the 7th day. No statistical difference was found between the gene expression at 1 and 3 days post-transfection. *$p<0.001$. $n=5$ in each group. US: ultrasound; MB: microbubble (Optison).